LOCKHEED MARTIN ENERGY RESEARCH LIBRARIES
3 4456 0515048 5

CENTRAL RESEARCH LIBRARY
DOCUMENT COLLECTION

cy. 2

ORNL-4752
UC-80 – Reactor Technology

OAK RIDGE NATIONAL LABORATORY
CENTRAL RESEARCH LIBRARY
DOCUMENT COLLECTION
LIBRARY LOAN COPY
DO NOT TRANSFER TO ANOTHER PERSON
If you wish someone else to see this document, send in name with document and the library will arrange a loan.
UCN-7969 (8 3-67)

THE EFFECT OF LIGHT-WATER REACTOR FUEL ROD FAILURE ON THE AREA AVAILABLE FOR EMERGENCY COOLANT FLOW FOLLOWING A LOSS-OF-COOLANT ACCIDENT

P. L. Rittenhouse
D. O. Hobson
R. D. Waddell, Jr.

OAK RIDGE NATIONAL LABORATORY
operated by
UNION CARBIDE CORPORATION
for the
U.S. ATOMIC ENERGY COMMISSION

Printed in the United States of America. Available from
National Technical Information Service
U.S. Department of Commerce
5285 Port Royal Road, Springfield, Virginia 22151
Price: Printed Copy $3.00; Microfiche $0.95

This report was prepared as an account of work sponsored by the United States Government. Neither the United States nor the United States Atomic Energy Commission, nor any of their employees, nor any of their contractors, subcontractors, or their employees, makes any warranty, express or implied, or assumes any legal liability or responsibility for the accuracy, completeness or usefulness of any information, apparatus, product or process disclosed, or represents that its use would not infringe privately owned rights.

ORNL-4752

Contract No. W-7405-eng-26

METALS AND CERAMICS DIVISION

THE EFFECT OF LIGHT-WATER REACTOR FUEL ROD FAILURE ON THE AREA AVAILABLE FOR EMERGENCY COOLANT FLOW FOLLOWING A LOSS-OF-COOLANT ACCIDENT

P. L. Rittenhouse D. O. Hobson
R. D. Waddell, Jr.

JANUARY 1972

OAK RIDGE NATIONAL LABORATORY
Oak Ridge, Tennessee 37830
operated by
UNION CARBIDE CORPORATION
for the
U.S. ATOMIC ENERGY COMMISSION

LOCKHEED MARTIN ENERGY RESEARCH LIBRARIES
3 4456 0515048 5

CONTENTS

Page

Abstract 1

Introduction 1

Experimental Details 6

Results 11

Comments on Individual Tests 17

Coolant Channel Blockage Distribution 27

Discussion 34

The Effect of Bundle Size on Test Results 34

Relationship Between Coolant Channel Blockage and C_c 43

Relationship Between Coolant Channel Blockage and Test Conditions 48

Coolant Channel Blockages in Reactor Fuel Assemblies 49

Conclusions and Recommendations 54

Acknowledgments 56

Appendix

Simplified Coolant Channel Blockage Analysis 57

THE EFFECT OF LIGHT-WATER REACTOR FUEL ROD FAILURE ON THE AREA AVAILABLE FOR EMERGENCY COOLANT FLOW FOLLOWING A LOSS-OF-COOLANT ACCIDENT

P. L. Rittenhouse D. O. Hobson
R. D. Waddell, Jr.

ABSTRACT

We have performed a series of temperature transient burst tests on bundles of simulated light-water reactor fuel rods. These experiments were conducted with rod internal pressures ranging from 100 to 1200 psig and heating rates from 10 to 100°F/sec. The major intent of this program was to ascertain the degree of coolant channel blockage that would be provided by fuel rod deformation and rupture during the loss-of-coolant accident postulated for light-water reactor systems.

The blockages measured in our multirod experiments were somewhat lower than those which can be predicted on the basis of swelling data for Zircaloy cladding tubes. This result is explainable in terms of interference between simultaneously deforming adjacent rods, some randomness of the axial position of maximum deformation and rupture, and test configuration.

On the basis of our results we have proposed criteria, related primarily to fuel rod internal pressure, for analysis and prediction of blockages produced in the reactor core by deformation of the fuel rods. Depending on reactor operating history and conditions and the severity of the loss-of-coolant accident, coolant channel blockages could range from essentially zero in some cases to almost 100% over appreciable portions of the core in others.

INTRODUCTION

The most serious accidents considered credible in light-water reactors (LWR's) are those associated with the breach of one of the many pipes in the primary coolant system. These postulated accidents, the loss-of-coolant accidents (LOCA's), would result in loss of pressure and expulsion of the reactor coolant. They could range in severity from a small leak to a double-ended rupture of the largest pipe in the system.

On loss of the coolant, redistribution of the heat stored in the fuel would raise the temperature of the fuel cladding quite rapidly. At a somewhat later time the decay heat from the fission products would be the dominant heat source and, if the temperature exceeds certain limits, the exothermic reaction between cladding (Zircaloy) and steam would also provide thermal energy.

Although the probability of any LOCA is considered to be small and that of the most severe LOCA extremely small, their consequences could be quite severe. Therefore, safeguards such as emergency core cooling systems (ECCS's) are engineered into LWR's to provide temperature transient termination and post-accident cooling for the reactor core and to minimize damage to the total reactor system. This is not to say, however, that no damage will result from a LOCA. Even with the ECCS operating near design capacity, portions of the reactor core may reach temperatures sufficient to allow deformation (swelling) and rupture of fuel rods. Deformation and rupture will occur when the stress provided by the internal pressure of fission gases (generated and collected in the fuel rods during normal operation) exceeds the yield and rupture strength of the cladding tubes. For purposes of reference, the stress on the cladding may be taken as about 8 times the internal fission gas pressure. Pressures in boiling-water reactor (BWR) fuel rods are usually below 200 psig even toward end of life; pressures in pressurized-water reactor (PWR) fuel rods at end of life may be in excess of 2000 psig. As examples, rupture temperatures of about 1700, 1400, and 1250°F are associated with internal pressures of 200, 500, and 1000 psig, respectively.[1] Of course, during normal reactor operation the cladding is at much lower temperatures and has considerably greater strength. Also, the pressure difference across the wall of the cladding tube is balanced or — most often — exceeded by the system pressure. The LOCA removes both of these limits and leads to cladding swelling and rupture.

When the fuel cladding ruptures the gaseous and volatile fission products occupying the free volume within the fuel rods are released to

---

[1]R. D. Waddell, Jr., and P. L. Rittenhouse, High-Temperature Burst Strength and Ductility of Zircaloy Tubing, ORNL-TM-3289 (March 1971).

the primary system and — as breach of the primary system was the event that initiated the LOCA — to the reactor containment. The containment is equipped with a number of fission product removal systems (i.e., sprays and filters) to prevent radioactive species from escaping to the outside environment. Although retention of radioactivity within the reactor system, preferably within the fuel rods, is the major overall concern for the accident, in this report we shall be more directly interested in fuel rod deformation and rupture with respect to its mechanics, its location within the core, and its effect on the failure of adjacent rods and blockage of passageways for emergency coolant flow.

The deformation (swelling) of the fuel rods prior to rupture can be considerable,[2,3] and it should be expected that the cross-sectional area available for coolant flow (coolant channel area) through fuel bundles will be restricted to some degree during the LOCA. Reduction in coolant channel area as a function of fuel cladding swelling can be easily calculated. The original coolant channel area (A_0) per fuel rod in an undeformed assembly is

$$A_0 = p^2 - 4[\tfrac{1}{4}(\pi d_0^2/4)] = p^2 - \pi d_0^2/4 , \qquad (1)$$

where

$p \equiv$ fuel rod pitch or rod center-to-center distance on a square array,

and

$d_0 \equiv$ original diameter of a fuel rod.

As the fuel rods swell — and here we shall assume that each swells uniformly and equally about its center and at the same axial location or elevation — the area for coolant flow, A, is reduced ($A < A_0$). At any time before adjacent rods touch — which occurs when the pitch, p, equals the diameter, d, of the swollen rods — the fraction of original coolant channel area blocked, F_A, can be calculated from the expression:

---

[2]P. L. Rittenhouse, Progress in Zircaloy Cladding Failure Modes Research, ORNL-TM-3188 (December 1970).

[3]D. O. Hobson and P. L. Rittenhouse, Deformation and Rupture Behavior of Light-Water Reactor Fuel Cladding, ORNL-4727 (September 1971).

$$F_A = (A_0 - A)/A_0 = \left[A_0 - \left(p^2 - \frac{\pi d^2}{4}\right)\right] \Big/ A_0 = \frac{\pi}{4}\left(d^2 - d_0^2\right) \Big/ A_0 \,, \quad (2)$$

where

$d \equiv$ diameter of swollen rods, and

$p \geq d \geq d_0$.

For fuel rod expansion with $d > p$, one or more assumptions must be made to permit calculation of F_A. In our case we shall assume that at $F_A = 1$ (total blockage) the rod cross section will be square. The length, ℓ, of the sides of the square, will be identical to the fuel rod pitch, $p = \ell$. An equivalent circumferential expansion (in percent) of the rods at $F_A = 1$ can be calculated from

$$\epsilon_c = 100 \times \left(\frac{4\ell - \pi d_0}{\pi d_0}\right) . \quad (3)$$

For expansions such that $4\ell > \pi d > \pi p$, both the coolant flow area, A, and the equivalent circumference of the rods are easily found by graphical methods. The results of determination of coolant channel blockage as a function of the expansion of an array of rods are presented in Fig. 1 for BWR and PWR rods of nominal dimensions. Notice that in both cases adjacent rods touch at just over 30% expansion [Eq. (2) can be used up until this point] and that total blockage is predicted at about 70% expansion. Other methods of calculation have been tried and all predict total blockage at expansions ranging from 60 to 75%. The method described here seems the most reasonable and realistic.

Using Fig. 1 and the expansion results for single tubes tested under temperature transient conditions,[3] we can generate the curve shown in Fig. 2. This curve predicts coolant channel blockage as a function of the maximum internal pressure achieved in the fuel rods prior to rupture. The data range shown encompasses the effects of heating rate and cladding wall-thickness variations.[3] With fuel rod internal pressures of 200 psig the blockage predicted is in the range 75 to 100%; at 500 psig, 40 to 65%; and at 1000 psig, 90 to 100%. These blockages must be considered as the maximum possible under the stated pressures. Factors such as nonuniformity of swelling, randomness of axial position of deformation,

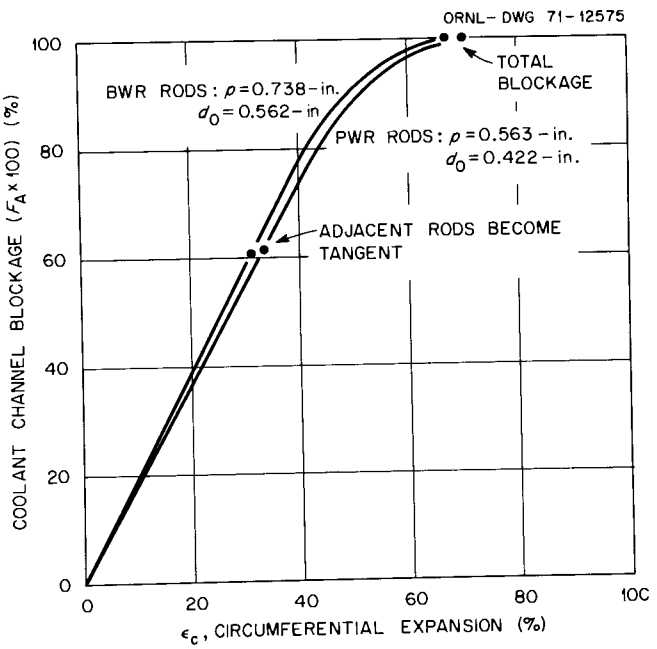

Fig. 1. Coolant Channel Blockage as a Function of Cladding Expansion. The percentage coolant channel blockage ($F_A \times 100$) resulting from a specified circumferential expansion, ϵ_c, is shown for both BWR- and PWR-size cladding. F_A versus ϵ_c is linear until adjacent rods touch (just over 30% expansion). Total blockage, $F_A = 1.0$, is predicted at about 70% expansion.

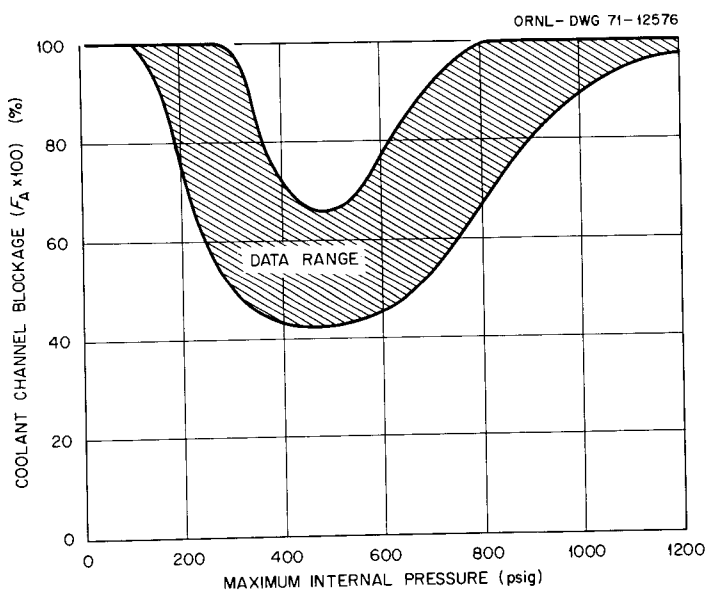

Fig. 2. Coolant Channel Blockage as a Function of Internal Pressure. These blockages were calculated on the basis of expansion data obtained in tests with single rods at internal pressures from 50 to 1200 psig and heating rates from 10 to 100°F/sec. The data range reflects the effects of heating rate and wall-thickness variations as well as normal experimental scatter.

rod-to-rod interference, test and fuel assembly configuration, and irradiation should tend to result in blockages of lesser degree than shown in Fig. 2. It is the purpose of this report to show these effects and to derive new blockage curves related to these factors.

EXPERIMENTAL DETAILS

Temperature transient tube burst tests were conducted on bundles of simulated fuel rods consisting of 13 Zircaloy tubes of BWR-size and on both 16- and 32-rod assemblies of PWR-size cladding. All of the BWR-size tubing (0.562 in. OD by 0.032 in. wall) was Zircaloy-4 purchased to ASTM specifications from Amax Specialty Metals, Inc. (AMAX). Some of the PWR-size cladding used was purchased from AMAX and the remainder was supplied by Westinghouse, Babcock & Wilcox, and Combustion Engineering. The outside diameter of these tubes (all Zircaloy-4) ranged from 0.420 to 0.439 in.; the wall thickness on all PWR tubes was nominally 0.027 in.

The simulated fuel rods consisted of 2-ft lengths of the Zircaloy cladding containing 16-in.-long quartz-encapsulated, tungsten heaters rated at about 3000 W each. Commercially built heaters were used in the tests with BWR-size rods and similar heaters were constructed in-house for the PWR tests. The power leads to each heater entered through 1/4 in.-diam stainless steel tubes in each end of the test rod. These tubes were welded to stainless steel fittings that threaded into Zircaloy end plugs (see schematic in Fig. 3). The stainless steel tubes also provided the ports for internal pressurization of the rods. Annealed copper gaskets were used to make pressure-tight seals between the Zircaloy end plugs and the stainless steel fittings. The power leads exited through Teflon seals in compression fittings on the stainless steel tubing.

After the rods were constructed and tested for electrical continuity, shorts, and leak tightness, they were assembled into bundles of the desired number of rods. In all cases the rods were arranged in a square array or grid with pitch characteristic of either a BWR or PWR fuel assembly. A schematic of the bundle in position in the experiment container is shown in Fig. 4. The container (preheat furnace) allowed the

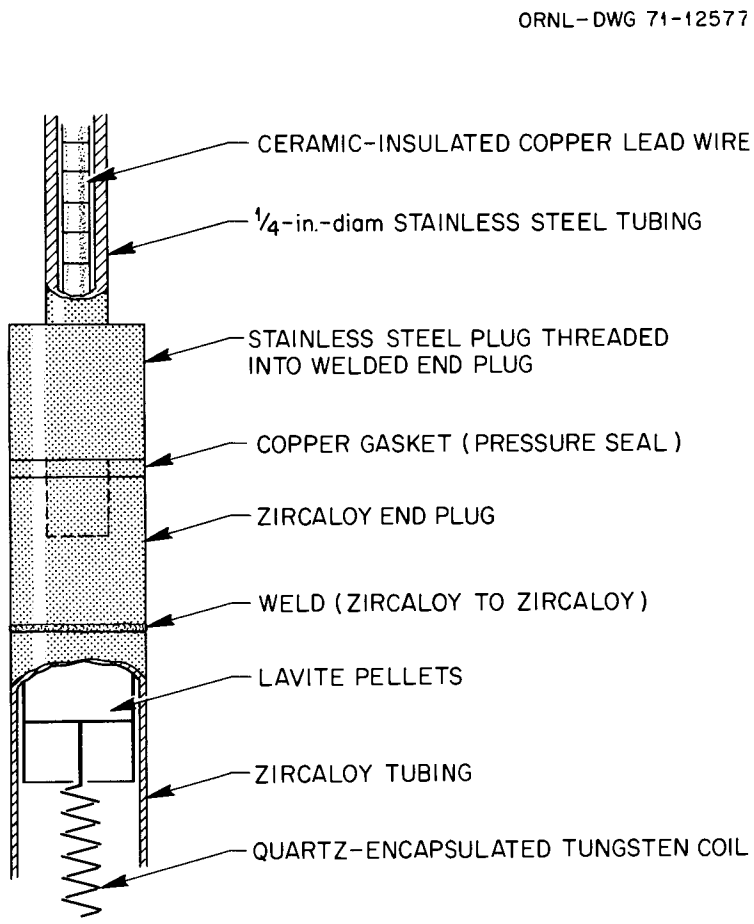

Fig. 3. Schematic of Simulated Fuel Rod Construction. This figure shows the details of heater, end plug, and pressure and power input line construction.

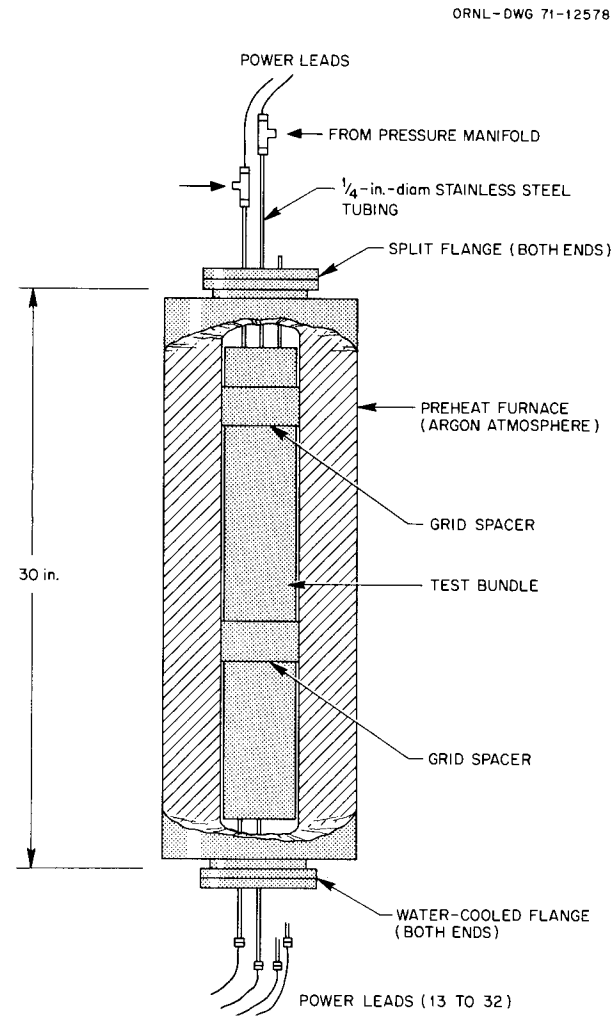

Fig. 4. Multirod Test Chamber. This schematic shows the test bundle in place in the experiment chamber.

rods to be preheated to nominal reactor operating temperature (about 600°F) in an environment of argon slightly in excess of atmospheric pressure. The stainless steel tubes (containing the power leads and providing the internal pressurization) connected to each of the simulated fuel rods exited the container through split flanges on each end. Grid spacers were used in all of the PWR tests and in the final BWR experiment to provide alignment and positioning of the rods. Figure 5 shows, schematically, the character of these grids. They are assembled by tack welding about 2-in. wide by 0.014-in.-thick stainless steel sheets into a square grid. Tabs punched into the surface of the stainless steel sheet give automatic alignment (the proper pitch) for the rods. Also shown in Fig. 5 are the dimensions of the fitted sleeve, sized to duplicate the cross-sectional area associated with 32 rods in a PWR fuel assembly.

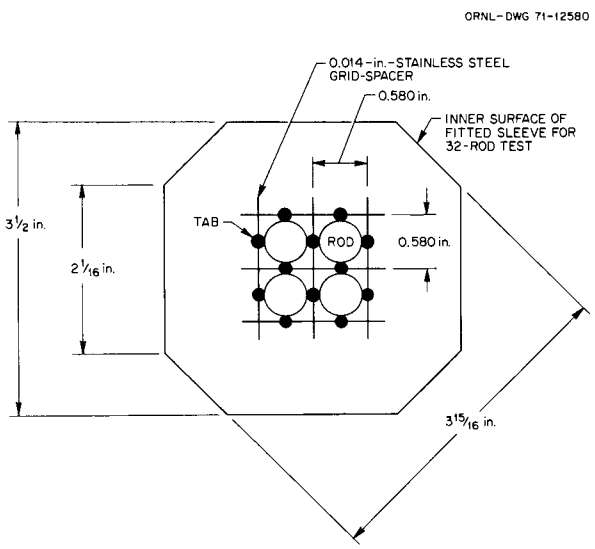

Fig. 5. Grid Spacer and Sleeve Dimensions. The dimensions of the fitted sleeve of the 32-rod tests are shown as well as information on grid-spacer construction.

When the test bundle reached the desired temperature, the rods were filled to pressures characteristic of those provided by fission product gases. (Internal pressures in our tests have ranged from 100 to 1200 psig. Pressures slightly greater than 2000 psig may be achieved in end-of-life PWR fuel rods.) Pressurization was accomplished using the manifold configuration shown in Fig. 6. High-purity argon was bled to the four identical legs of the manifold. Each leg contained eight ports and valves for pressurizing individual specimens. When pressurization was complete the specimens were valved off and the transient burst test was initiated. The desired temperature transient (a linear heating rate in the range 10 to 100°F/sec) was programmed by a Model FGE 5110 Data-Trak (Research, Inc. instrument). Power and temperature control were provided (see Fig. 7)

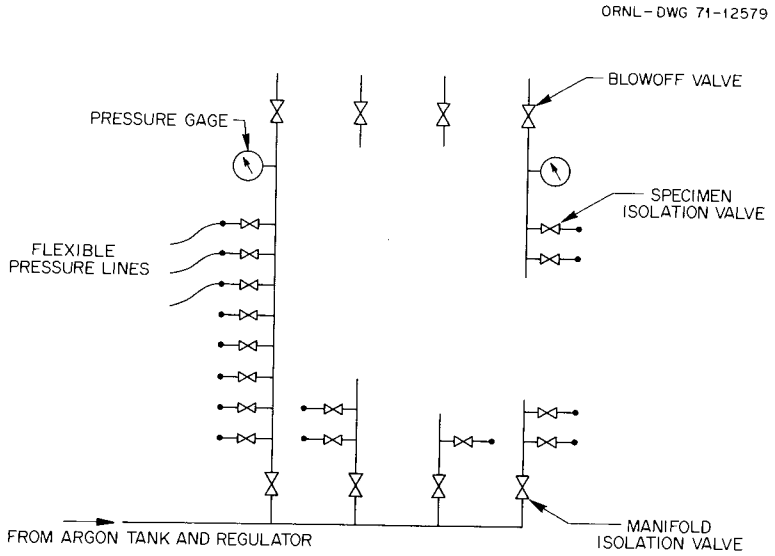

Fig. 6. Schematic of Pressurization Manifold. The valves, lines, and gages comprising the pressurizing manifold used in the multirod tests are shown in this diagram.

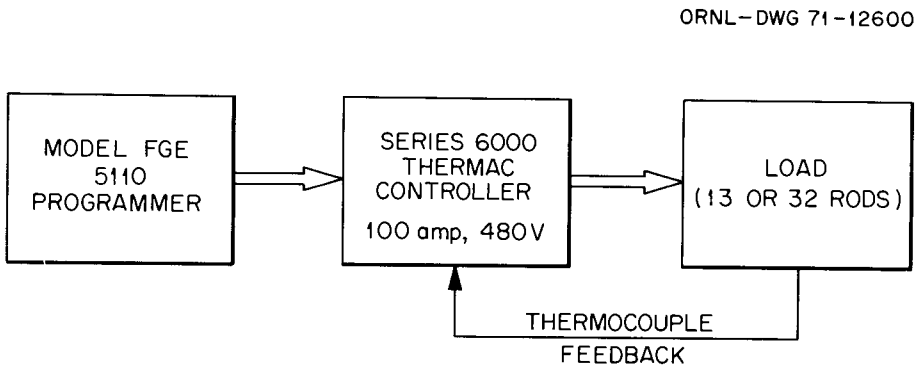

Fig. 7. Programming and Control System. This simple diagram shows the combination of programming, control, and feedback systems used in obtaining transient heating conditions.

by a Series 6000 Thermac (Research, Inc.) rated at 100 A and 480 V. The heaters are wired in parallel and were individually fused. The temperature transient was allowed to proceed until all the rods ruptured, until the fuses protecting the silicon-controlled rectifiers of the Thermac blew, or until a "scram" button was hit. All of these cases were experienced.

The instrumentation of a 13-rod bundle consisted typically of six Chromel-P–Alumel thermocouples and four pressure cells; eight thermocouples and four pressure cells were used in the 32-rod tests. (Thermocouple and pressure cell positions will be described later for individual tests.) Signals from the thermocouples and pressure cells were fed through an analog computer (to remove noise) to a fast-response multichannel recorder. Thermocouple junctions were made by spot welding the wires to tantalum pads attached (spot welded) to the cladding surface. Tantalum tabs (about 1/5 the length of tubing circumference) were used to strap the thermocouples to the rods.

After completion of the burst test the entire bundle was cast in epoxy, sectioned at several (up to 14) axial positions, and the sections polished. The method of measuring remaining coolant channel area depended upon the test configuration. For instance, the cross section of the container for the 13-rod tests was circular and of greater area than that associated with 13 rods in a BWR fuel assembly. Therefore, some amount of unrestrained bowing of the rods occurred. Because of this the following procedure was used. The cross-sectional area of each of the deformed rods was measured using a planimeter on photographs of the sections. Referring to Fig. 8, it is clear that the area of each full coolant channel, channels 1–4, is A_0 (as defined earlier) and that of the half channels, 5–12, is $A_0/2$. To find the coolant channel area reduction of one of the full channels, say channel 1, we would sum the areas of deformed tubes 2, 4, 5, and 7 ($a_2 + a_4 + a_5 + a_7 = \bar{a}$) and calculate F_A as

$$F_A = \left[A_0 - \left(p^2 - \frac{\bar{a}}{4}\right)\right] \Big/ A_0 = \left(\frac{\bar{a} - \pi d_0^2}{4}\right) \Big/ A_0 \ . \tag{4}$$

The reduction in coolant channel area for the entire cross section, $\bar{F}_A$, is simply the weighted average of that for the individual channels and half channels. In the 32-rod tests in which fitted sleeves were used (see Fig. 5, p. 8), planimeter measurements of channel areas can be made directly on all 21 full channels and F_A calculated by

$$F_A = (A_0 - A')/A_0 \ , \tag{5}$$

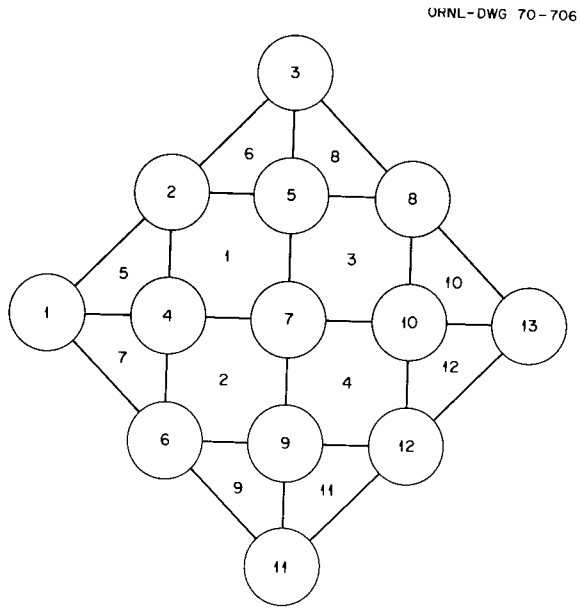

Fig. 8. Rod and Channel Identification. The circles represent the 13 Zircaloy rods of the burst test assembly. The four full coolant channels are numbered 1 through 4 and the eight half channels 5 through 12.

where A′ is the planimeter measurement of the coolant channel area remaining. Again, F_A for the entire cross section ($\overline{F}_A$) is the average of those for the individual channels.

In some of the more highly deformed cross sections, considerable distortion of the original grid occurred (i.e., the grid area, G_A, of individual channels was greater or less than the original grid area given by p^2). Planimeter measurement of the new grid area permits calculation of a modified fractional area blockage, F'_A, as

$$F'_A = \frac{\left[G_A - \left(\pi d_0^2/4\right)\right] - A'}{\left[G_A - \left(\pi d_0^2/4\right)\right]} = \frac{A'_0 - A'}{A'_0} . \qquad (6)$$

RESULTS

The nominal experimental conditions and configurations of the 11 multirod tests are shown in Table 1. The first column gives the test number, the second the nominal internal pressure (at about 600°F) of the rods (pressure usually increased about 10% during the transient), and the third the nominal heating rate (experimentally within ±10%). Columns 4, 5, and 6 of Table 1 refer to the test configurations.

Figure 9 is a schematic of the instrumentation layout for the 13-rod tests. Tubes representative of each of the four unique positions in the bundle were monitored for temperature and internal pressure. The first position, rod 7, was fitted with a pressure cell and a thermocouple

Table 1. Test Conditions and Configuration

Test Number	Nominal Internal Pressure (psig)	Nominal Heating Rate (°F/sec)	Number of Rods	Rod Type	Bundle Container	Comments
1	300	100	13	BWR	Circular[a]	Three of the rods lost pressure and did not deform. Average rod rupture temperature (T_R), 1740°F.
2	200	100	13	BWR	Circular	T_R = 1850°F.
3	400	100	13	BWR	Circular	T_R = 1720°F.
4	400	25	13	BWR	Circular	Two rods lost pressure. T_R = 1770°F.
5	200	25	13	BWR	Circular	T_R = 1790°F.
6	100	50	13	BWR	Circular	Two rods did not rupture because of partial pressure loss. T_R > 2100°F.
7	200	10	32	PWR	Circular	T_R ~ 1800°F. Some eutectic formation.
8	200	90	16	PWR	Square (fitted)[b]	T_R ~ 1800°F.[c]
9	700	10	32	PWR	Octagonal (fitted)[b]	T_R ~ 1550°F.[d]
10	1000	25	32	PWR	Octagonal (fitted)[b]	T_R ~ 1475°F.[e]
11	1200	25	16	PWR	Square (fitted)	T_R ~ 1400°F.[c]

[a]Cross section of container of greater area than that associated with 13 rods of BWR configuration or, for test 7, with 32 rods of PWR configuration.

[b]Fitted containers have cross-sectional area equivalent to that associated with the simulated PWR assembly.

[c]Tests to be analyzed by Combustion Engineering, Inc., Windsor, Conn.

[d]Two rods unheated and unpressurized; eight rods did not rupture.

[e]Two rods unheated; 16 rods ruptured while 9 others deformed appreciably (20 to 50%) but did not rupture; 7 rods deformed only slightly (0 to 20%).

at the center of the heated length of the bundle. The second position is a circle comprised of rods 4, 5, 9, and 10. One of these rods had a pressure cell and two thermocouples – one 4 in. above the center of the heated length and one 4 in. below. The third position, bolt circle containing rods 2, 6, 8, and 12, was instrumented as the first position and the fourth position (rods 1, 3, 11, and 13) as the second.

The temperature distribution in the 13-rod bundles during the tests is typified by that measured in tests 2 and 3. Position 2 thermocouples registered a 30°F temperature difference (axial ΔT) over an 8 in. span; the highest temperature was approximately at the center of the bundle

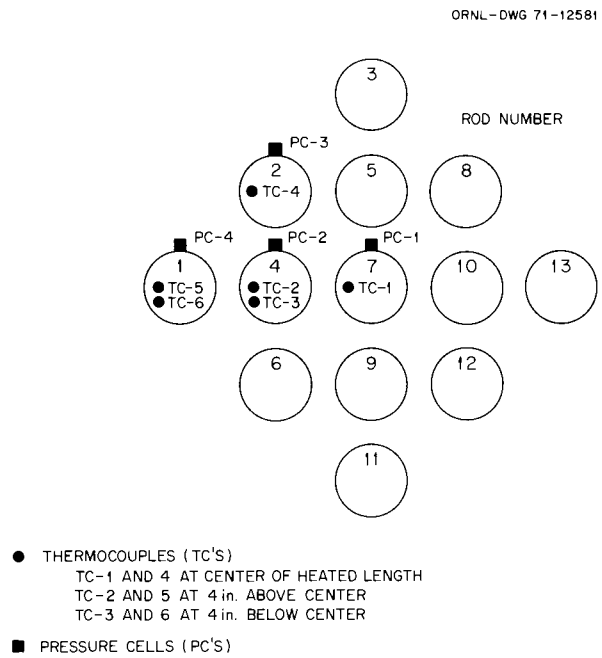

Fig. 9. Instrumentation for 13-Rod Tests. This figure shows the position of thermocouple (TC-1 through TC-6) and pressure cell installation. Rods 4, 5, 9, and 10 are of equivalent position as are 2, 6, 8, 12, and 1, 3, 11, 13.

while the lowest was 4 in. above center. (The position of maximum blockage corresponded to the highest temperature position in all tests except those where the grid was centered in the hot zone.) The temperature drop across these bundles (radial ΔT) from positions 1 to 3, was about 15°F while that from positions 1 to 4 was about 60°F. Both the axial and radial ΔT's changed with time during the experiments and those quoted above are for a time approximately 1 to 2 sec before cladding rupture.

The positions of the thermocouples in test bundles 7, 9, and 10 (32-rod tests) are given in Fig. 10. In each case, temperatures were monitored over at least 8 in. of bundle length. Test 7 (nominal heating rate of 10°F/sec) had an overall bundle average heating rate of 8.0°F/sec. Heating rate in the center of the bundle, as indicated by thermocouple 2, was 8.6°F/sec. The radial temperature gradient, from center to outside of the assembly of rods, approached 200°F at a temperature of 1700°F whereas the axial temperature gradients were somewhat less, as shown

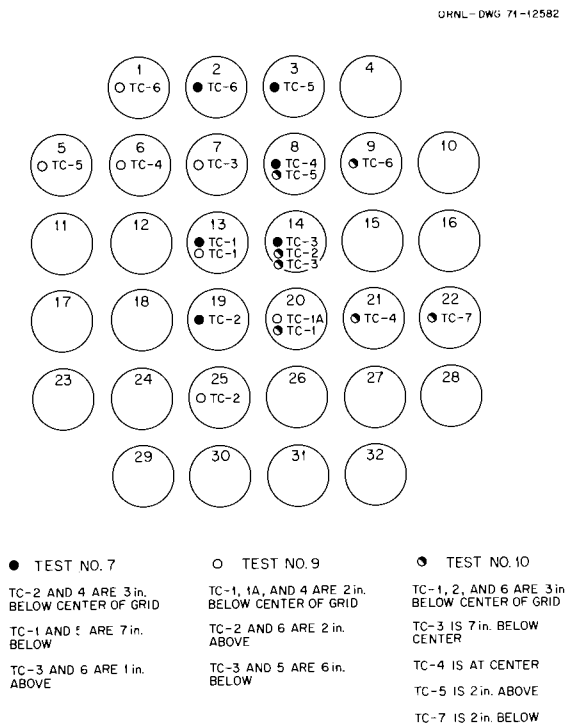

Fig. 10. Thermocouple Positions in the 32-Rod Tests. The rods to which thermocouples were attached and the axial position of the thermocouples are shown for tests 7, 9, and 10.

in Table 2, and most of the temperature difference was in the 3- to 7-in. interval below the center of the grid spacer.

The average heating rate during test 9 (determined from thermocouples 1, 2, 4, and 6) was 8.2°F/sec (see Table 3). (Extrapolation of the linear portions of the heating curves back to the starting temperature gives the time corrections listed in the table footnotes.) Because of the "dead" or unheated rods (7 and 9) the temperature distribution across the bundle was skewed slightly (e.g., the temperature on rod 25 was higher than that indicated on rod 13). Radial temperature gradients in the bundle, as shown in Table 4, were somewhat lower than those for test 7. The axial gradient in the 4-in. length spanning the grid spacer was only 30°F, but the temperature 6 in. below the grid was quite low.

Tables 5 and 6 give the temperature history and gradients in test 10. These data show that the temperature uniformity in this test was by far the best of any experiment run. This was not accidental but the result of improvements in heater construction and positioning within the tubes.

Table 2. Temperature Gradients in Test Bundle 7

Time (sec)	Gradients,[a,b] °F										
	Radial			Axial							
	ΔT_1	ΔT_2	ΔT_3	ΔT_4	ΔT_5	ΔT_6	ΔT_7	ΔT_8	ΔT_9	ΔT_{10}	ΔT_{11}
0[c]	+3	+22	−14	−43	−39	−79	−40	−43	−21	−22	−36
5	+11	+28	−18	−51	−40	−97	−57	−68	−42	−11	−29
10	0	+42	−14	−30	−40	−86	−46	−46	−4	−26	−40
30	+58	+56	0	0	0	−56	−56	−112	−58	+58	+58
45[d]	+72	+83	+21	+44	+40	−18	−58	−130	−47	+91	+112
60	+86	+122	+95	+40	+81	+13	−68	−154	−32	+72	+167
70	+81	+134	+108	+51	+92	+25	−67	−148	−14	+65	+173
80	+83	+160	+138	+62	+108	+40	−68	−151	+9	+53	+199
90[e]	+83	+162	+112	+65	+83	+25	−58	−141	+21	+54	+163
100	+83	+144	+126	+79	+93	+61	−32	−115	+29	+49	+176
110	+68	+168	+164	+88	+122	+66	−36	−104	+62	+26	+190
120[f]	+86	+198		+94			−18	−104	+94	0	

[a] ΔT_1 is temperature difference between TC-2 and TC-4 (see Fig. 10 for thermocouple positions). ΔT_2 = (TC-3)−(TC-6), ΔT_3 = (TC-1)−(TC-5).

[b] ΔT_4 = (TC-5)−(TC-6), ΔT_5 = (TC-1)−(TC-2), ΔT_6 = (TC-1)−(TC-3), ΔT_7 = (TC-2)−(TC-3), ΔT_8 = (TC-4)−(TC-3), ΔT_9 = (TC-4)−(TC-6) ΔT_{10} = (TC-5)−(TC-4), ΔT_{11} = (TC-1)−(TC-4).

[c] Average center line temperature at time zero, T_{c0}, equals 770°F.

[d] T_{c45} = 1135°F.

[e] T_{c90} = 1440°F.

[f] T_{c120} = 1710°F.

Table 3. Temperature History of Test Bundle 9

Time (sec)	Temperature, °F, and Heating Rate, °F/sec, to the Indicated Temperature					
	TC-1[a]	TC-2	TC-3	TC-4	TC-5	TC-6
0	545	545	525	575	545	555
20	612	600	545	655	555	600
	3.4	2.8	1.0	4.0	0.5	2.2
40	720	723	555	768	575	705
	4.4	4.5	0.8	4.8	0.8	3.8
60	871	895	586	930	620	863
	5.5	5.8	1.0	5.9	1.2	5.1
80	1030	1060	630	1085	668	1000
	6.1	6.4	1.3	6.4	1.5	5.6
100	1186	1205	720	1222	725	1135
	6.4	6.6	2.0	6.5	1.8	5.8
120	1380	1382	820	1380	820	1304
	7.0	7.0	2.5	6.7	2.3	6.2
130	1460	1492	910	1440	892	1355
	7.0	7.3	3.0	6.7	2.7	6.2
135	1525	1545	1000	1525	940	1437
	7.3[b]	7.4	3.5	7.0[c]	2.9	6.5
140	1497	1572	1060	1492	980	1490
		7.3[d]	3.8		3.1	6.7[e]

[a] Position of thermocouple (TC) is as given in Fig. 10.

[b] Linear rate of 8.3°F/sec extrapolates to 15 sec.

[c] Linear rate of 7.7°F/sec extrapolates to 9 sec.

[d] Linear rate of 8.6°F/sec extrapolates to 13 sec.

[e] Linear rate of 8.3°F/sec extrapolates to 13 sec.

Table 4. Temperature Gradients in Test Bundle 9

Time (sec)	Radial Gradient,[a] °F		Axial Gradient[b] (°F)
	ΔT_1	ΔT_2	
0	−30	−10	0
20	−43	0	+12
40	−48	+18	−3
60	−59	+22	−24
80	−55	+60	−30
100	−36	+70	−19
120	0	+78	−2
130	+20	+137	−32
135	0	+108	−20
140	+5	+82	−30

[a] ΔT_1 is temperature difference between TC-1 and TC-4 at ΔT_2 = (TC-2)−(TC-6). See Fig. 10 for thermocouple positions.

[b] (TC-1)−(TC-2).

Table 5. Temperature History of Bundle 10

Time (sec)	Temperature, °F, and Heating Rate, °F/sec, to the Indicated Temperature						
	TC-1[a]	TC-2	TC-3[b]	TC-4	TC-5	TC-6	TC-7
0	572	621		599	639	626	647
10	680	707		675	753	729	798
	10.8	8.6		7.6	11.4	10.3	15.1
20	1080	1080		1015	1080	1080	1173
	25.4	22.9		20.8	22.0	22.7	26.3
30	1296	c		1296	1296	1296	1284
	24.1	c		23.2	21.9	22.3	21.2
39	1517			1490	1514	1511	1476
	24.2			22.8	22.4	22.6	21.2
41	1576			d	1576	d	d
	24.6				22.8		

[a] Position of thermocouple (TC) is as given in Fig. 10.

[b] Thermocouple 3 became detached from tube surface prior to test run.

[c] Thermocouple 2 was lost at about 28 sec.

[d] Thermocouples 4, 6, and 7 were lost at about 40 sec.

Table 6. Temperature Gradients in Bundle 10

Time (sec)	Radial ΔT^a (°F)	Axial ΔT^b (°F)
0	−75	−67
10	−118	−73
20	−93	0
30	+12	0
39	+41	+3
41		0

[a]Temperature difference between TC-1 and TC-7.

[b]Temperature difference between TC-1 and TC-5.

Tables 7 and 8 show reduction in coolant channel area for individual channels, F_A, and the averages for the cross sections examined, $\overline{F}_A$. The maximum $\overline{F}_A$ observed, 0.84, was in test 6 (100 psig) and the minimum, 0.21, in test 3 (400 psig).

Comments on Individual Tests

Test 1 was run with an internal pressure of 300 psig (at 600°F) at a nominal heating rate of 100°F/sec (measured as about 95°F/sec). Three of the 13 rods (rods 1, 11, and 13) lost pressure during the experiment and, therefore, neither deformed appreciably nor ruptured. Average failure temperature of the remaining ten rods was about 1740°F with the rods at an internal pressure of 315 psig. Posttest views of the deformed bundle and three cross sections are given in Figs. 11 and 12, respectively.

In test 2 the heating rate was again about 95°F/sec. The internal pressure was 200 psig at 575°F and 205 psig just prior to rupture at 1850°F. All rods ruptured. Cross-sectional views of the bundle are shown in Fig. 13.

Both tests 3 and 4 were run with an internal pressure of 400 psig (575°F). Heating rates for the two were about 100 and about 25°F, respectively. Rupture of the rods in test 3 occurred at about 1720°F

Table 7. Coolant Channel Blockage in the 13-Rod BWR Tests

Test and Section Numbers	Distance from Axial Center (in.)	F_A^a Channel 1	2	3	4	5	6	7	8	9	10	11	12	$\bar{F}_A^b$
1-1A	−4.75	0.19	0.21	0.43	0.33	0.13	0.35	0.26	0.35	0.24	0.54	0.10	0.55	0.30
1-2B	−3.75	0.50	0.30	0.69	0.29	0.25	0.71	0.26	0.81	0.40	0.39	0.38	0.19	0.45
1-3B	−0.50	0.54	0.49	1.00	0.48	0.27	0.15	0.27	0.63	0.06	1.00	0.06	0.62	0.50
1-5A	0.00	0.20	0.59	0.20	0.19	0.05	0.21	0.46	0.21	0.77	0.04	0.37	0.05	0.28
2-3A	−3.15	0.43	0.44	0.18	0.27	0.97	0.17	0.99	0.17	0.17	0.23	0.26	0.34	0.37
2-3B	−2.25	0.68	0.33	0.50	0.34	0.58	0.85	0.25	0.68	0.41	0.39	0.42	0.25	0.47
2-5A	−1.50	0.56	0.61	0.26	0.48	1.00	0.38	1.00	0.31	0.43	0.23	0.52	0.43	0.51
2-5B	0.00	0.61	0.62	0.81	0.81	0.21	0.47	0.24	0.41	0.44	0.77	0.37	0.79	0.59
2-7A	+2.25	0.12	0.15	0.21	0.21	0.19	0.13	0.18	0.20	0.22	0.28	0.25	0.24	0.19
3-4A	−1.75	0.27	0.10	0.27	0.13	0.11	0.49	0.09	0.48	0.24	0.12	0.15	0.14	0.21
3-5A	−0.75	0.11	0.12	0.26	0.29	0.11	0.12	0.12	0.11	0.18	0.43	0.18	0.45	0.21
3-6A	0.00	0.08	0.09	0.09	0.10	0.07	0.12	0.08	0.12	0.12	0.10	0.10	0.11	0.10
3-7A	+0.30	0.27	0.27	0.25	0.26	0.31	0.27	0.31	0.15	0.17	0.15	0.15	0.16	0.21
3-8A	+1.75	0.28	0.26	0.24	0.25	0.13	0.11	0.11	0.08	0.15	0.08	0.15	0.09	0.21
4-2A	−2.50	0.22	0.26	0.13	0.15	0.37	0.11	0.33	0.13	0.17	0.15	0.17	0.15	0.20
4-3A	−1.85	0.15	0.30	0.33	0.26	0.17	0.25	0.29	0.35	0.31	0.46	0.18	0.35	0.28
4-3B	−1.25	0.20	0.25	0.24	0.25	0.27	0.20	0.29	0.21	0.40	0.26	0.38	0.25	0.26
4-6A	0.00	0.20	0.43	0.18	0.39	0.16	0.16	0.15	0.14	0.64	0.11	0.65	0.13	0.28
4-7A	+0.50	0.26	0.29	0.24	0.28	0.18	0.35	0.18	0.35	0.50	0.12	0.53	0.14	0.28
4-7B	+2.50	0.15	0.14	0.16	0.30	0.16	0.16	0.16	0.15	0.14	0.18	0.29	0.33	0.20
5-4A	−1.25	0.12	0.09	0.15	0.14	0.09	0.27	0.07	0.27	0.18	0.14	0.21	0.16	0.15
5-5A	−0.75	0.11	0.08	0.14	0.17	0.12	0.25	0.10	0.23	0.27	0.15	0.32	0.20	0.17
5-6A	0.00	0.18	0.13	0.22	0.35	0.28	0.40	0.26	0.36	0.24	0.23	0.37	0.38	0.27
5-6B	+0.75	0.62	0.59	0.55	0.69	0.48	0.25	0.36	0.12	0.28	0.43	0.32	0.47	0.48
5-7B	+1.25	0.54	0.68	0.70	0.70	0.53	0.11	0.56	0.19	0.37	0.73	0.31	0.63	0.54
5-8B	+1.75	0.55	0.81	0.67	0.69	0.55	0.08	0.66	0.20	0.52	0.63	0.40	0.50	0.56
5-9B	+2.25	0.25	0.56	0.28	0.43	0.25	0.03	0.39	0.06	0.54	0.26	0.41	0.24	0.32
6-2A	−4.40	1.00[c]	0.81	1.00	0.82	1.00	1.00	0.81	1.00	0.45	0.50	0.50	0.60	0.82
6-3B	−3.25	1.00	1.00	1.00	0.76	0.56	1.00	1.00	0.97	0.82	0.42	0.48	0.47	0.84
6-5B	+2.75	0.66	0.71	0.77	0.80	0.59	1.00	0.53	1.00	0.78	0.92	0.70	0.84	0.76
6-6B	+3.50	0.66	0.61	0.74	1.00	0.44	0.69	0.45	0.67	0.74	1.00	1.00	1.00	0.74
6-8A	+4.00	0.49	0.52	0.48	0.89	0.27	0.47	0.43	0.40	0.50	0.73	0.82	1.00	0.59

[a] Fractional reduction in coolant channel area for individual channels.

[b] Fractional reduction in coolant channel area, average for all channels.

[c] In most cases where F_A is shown as 1.00 the calculation gave a negative value (i.e., greater than total blockage). This is allowable only because of the appreciable bowing that occurred.

Table 8. Coolant Blockage in the 32-Rod PWR Tests

Test and Section Number	Axial Position (in.)	F_A[a] Channel 1	2	3	4	5	6	7	8	9	10	11	12	13	14	15	16	17	18	19	20	21	$\bar{F}_A$[b]
7-1	−4.0	0.02	0.01	0.01	0.02	0.01	0.01	0.03	0.03	0.01	0.01	0.01	0.02	0.00	0.00	0.01	0.03	0.03	0.01	0.03	0.00	0.00	0.01
7-2	−3.5	0.06	0.03	0.03	0.04	0.05	0.03	0.06	0.05	0.05	0.03	0.03	0.03	0.01	0.02	0.04	0.06	0.04	0.05	0.05	0.03	0.01	0.04
7-3	−3.0	0.05	0.05	0.05	0.05	0.05	0.08	0.08	0.08	0.07	0.06	0.04	0.07	0.04	0.06	0.07	0.11	0.06	0.08	0.08	0.07	0.04	0.06
7-4	−2.5	0.08	0.08	0.07	0.06	0.08	0.12	0.10	0.10	0.07	0.08	0.06	0.07	0.06	0.09	0.11	0.18	0.08	0.10	0.09	0.07	0.06	0.09
7-5	−2.0	0.12	0.13	0.21	0.09	0.10	0.23	0.30	0.17	0.08	0.11	0.18	0.02	0.08	0.13	0.17	0.23	0.25	0.16	0.11	0.06	0.07	0.14
7-6	−1.5	0.69	0.33	0.49	0.69	0.54	0.41	0.63	0.43	0.50	0.26	0.21	0.16	0.23	0.23	0.30	0.53	0.52	0.15	0.13	0.15	0.17	0.37
7-7	−1.0	0.82	0.83	0.64	0.57	0.68	0.56	0.87	0.50	0.58	0.63	0.24	0.17	0.39	0.27	0.42	0.66	0.38	0.29	0.16	0.24	0.35	0.49
7-8	−0.5	0.51	0.42	0.31	0.40	0.41	0.37	0.32	0.38	0.30	0.27	0.15	0.21	0.23	0.20	0.23	0.29	0.25	0.24	0.23	0.19	0.19	0.29
7-9	0.0[c]	0.38	0.18	0.24	0.40	0.30	0.20	0.17	0.38	0.30	0.20	0.17	0.21	0.22	0.20	0.14	0.29	0.17	0.25	0.23	0.24	0.19	0.24
7-10	+0.5	0.16	0.10	0.11	0.31	0.15	0.13	0.10	0.32	0.17	0.13	0.31	0.31	0.26	0.25	0.15	0.17	0.22	0.24	0.29	0.24	0.24	0.21
7-11	+1.0	0.10	0.07	0.07	0.19	0.11	0.10	0.09	0.21	0.11	0.12	0.24	0.28	0.31	0.28	0.14	0.16	0.12	0.26	0.25	0.17	0.23	0.17
7-12	+1.5	0.06	0.05	0.04	0.12	0.06	0.08	0.06	0.15	0.06	0.05	0.09	0.28	0.17	0.21	0.14	0.11	0.07	0.15	0.23	0.15	0.13	0.12
7-13	+2.0	0.03	0.03	0.02	0.05	0.03	0.05	0.03	0.08	0.03	0.03	0.02	0.19	0.08	0.07	0.07	0.05	0.03	0.08	0.22	0.03	0.05	0.06
7-14	+4.0	0.01	0.02	0.01	0.02	0.02	0.04	0.02	0.05	0.02	0.02	0.02	0.03	0.04	0.04	0.05	0.03	0.03	0.05	0.06	0.02	0.03	0.03
7-15	+4.5	0.04	0.03	0.02	0.04	0.05	0.05	0.03	0.04	0.05	0.01	0.02	0.04	0.04	0.04	0.04	0.02	0.03	0.05	0.11	0.03	0.03	0.04
7-16	+5.0	0.06	0.03	0.02	0.06	0.06	0.06	0.03	0.06	0.05	0.01	0.02	0.04	0.04	0.05	0.04	0.02	0.02	0.11	0.10	0.03	0.03	0.04
9-1	−5.0[d]	0.00	0.25	0.00	0.00	0.00	0.22	0.29	0.00	0.00	0.03	0.20	0.11	0.02	0.18	0.05	0.26	0.12	0.15	0.11	0.31	0.18	0.08
9-2	−4.5	0.06	0.26	0.06	0.00	0.02	0.30	0.16	0.00	0.05	0.01	0.32	0.23	0.00	0.21	0.11	0.17	0.24	0.11	0.16	0.34	0.25	0.13
9-3	−4.0	0.33	0.30	0.59	0.36	0.26	0.29	0.70	0.35	0.35	0.26	0.57	0.64	0.27	0.21	0.21	0.48	0.75	0.62	0.69	0.42	0.31	0.43[e]
9-4	−3.5	0.48	0.32	0.62	0.42	0.59	0.36	0.58	0.80	0.34	0.47	0.58	0.36	0.44	0.33	0.27	0.71	0.82	0.70	0.54	0.50	0.63	0.52
9-5	−3.0	0.50	0.45	0.72	0.54	0.77	0.61	0.35	0.55	0.72	0.67	0.44	0.18	0.61	0.56	0.43	0.43	0.40	0.27	0.12	0.65	0.57	0.50
9-6	−2.5	0.08	0.54	0.12	0.24	0.37	0.55	0.26	0.04	0.54	0.76	0.39	0.28	0.68	0.64	0.67	0.30	0.28	0.22	0.12	0.43	0.39	0.38
9-7	−2.0	0.00	0.00	0.00	0.08	0.00	0.33	0.14	0.00	0.02	0.14	0.23	0.16	0.11	0.31	0.28	0.23	0.20	0.15	0.06	0.20	0.27	0.12
9-8	−1.5	0.00	0.11	0.00	0.02	0.00	0.21	0.13	0.00	0.02	0.05	0.16	0.14	0.00	0.14	0.23	0.16	0.17	0.08	0.05	0.12	0.11	0.07
9-9	−1.0	0.00	0.14	0.00	0.03	0.00	0.19	0.09	0.00	0.00	0.05	0.16	0.05	0.00	0.09	0.19	0.11	0.15	0.04	0.02	0.07	0.11	0.05
9-10	+1.0	0.06	0.16	0.21	0.13	0.02	0.13	0.07	0.16	0.07	0.24	0.18	0.11	0.12	0.09	0.23	0.23	0.19	0.05	0.18	0.04	0.16	0.13
9-11	+1.5	0.17	0.27	0.40	0.23	0.11	0.19	0.09	0.24	0.17	0.40	0.18	0.15	0.00	0.28	0.19	0.26	0.20	0.00	0.24	0.10	0.24	0.19
9-12	+2.0	0.21	0.26	0.15	0.22	0.39	0.08	0.18	0.15	0.25	0.42	0.29	0.18	0.19	0.22	0.28	0.15	0.23	0.21	0.10	0.30	0.00	0.21
9-13	+2.5	0.42	0.34	0.63	0.26	0.24	0.18	0.00	0.31	0.28	0.58	0.15	0.23	0.49	0.43	0.02	0.25	0.15	0.00	0.35	0.09	0.30	0.26
10-1	+3.0[d]	0.15	0.13	0.14	0.09	0.15	0.15	0.19	0.12	0.14	0.18	0.18	0.13	0.13	0.12	0.15	0.19	0.28	0.08	0.13	0.12	0.09	0.15[f]
10-2	+2.5	0.18	0.11	0.17	0.13	0.11	0.13	0.18	0.13	0.13	0.19	0.12	0.18	0.10	0.10	0.13	0.23	0.28	0.09	0.20	0.23	0.15	0.15
10-3	+2.0	0.18	0.17	0.10	0.50	0.10	0.19	0.20	0.12	0.44	0.18	0.12	0.51	0.12	0.17	0.11	0.00	0.25	0.08	0.15	0.50	0.11	0.21
10-4	+1.5	0.13	0.21	0.12	0.61	0.14	0.17	0.13	0.10	0.52	0.15	0.08	0.55	0.09	0.14	0.10	0.15	0.15	0.06	0.12	0.56	0.08	0.21
10-5	−1.5	0.12	0.12	0.19	0.08	0.15	0.12	0.11	0.16	0.10	0.13	0.17	0.14	0.09	0.08	0.11	0.13	0.13	0.12	0.19	0.10	0.10	0.13
10-6	−2.0	0.39	0.45	0.36	0.19	0.29	0.36	0.36	0.33	0.18	0.22	0.26	0.41	0.16	0.16	0.28	0.22	0.20	0.25	0.66	0.23	0.15	0.29
10-7	−2.5	0.66	0.72	0.52	0.21	0.40	0.56	0.58	0.51	0.23	0.47	0.46	0.52	0.24	0.32	0.45	0.42	0.40	0.41	0.67	0.35	0.25	0.45
10-8	−3.0	0.53	0.62	0.50	0.62	0.67	0.38	0.72	0.81	0.35	0.49	0.65	0.84	0.35	0.45	0.49	0.54	0.79	0.62	0.67	0.84	0.43	0.58
10-9	−3.5	0.55	0.54	0.56	0.71	0.69	0.65	0.75	0.76	0.60	0.60	0.73	0.83	0.69	0.58	0.56	0.55	0.84	0.70	0.67	0.88	0.69	0.67
10-10	−4.0	0.81	0.79	0.84	0.51	0.82	0.88	0.69	0.71	0.64	0.59	0.77	0.56	0.78	0.80	0.75	0.51	0.43	0.55	0.55	0.50	0.81	0.68
10-11	−4.5	0.92	0.74	0.84	0.67	0.74	0.82	0.74	0.62	0.47	0.71	0.66	0.34	0.51	0.58	0.67	0.70	0.37	0.55	0.49	0.29	0.63	0.59
10-12	−5.0	0.50	0.77	0.57	0.23	0.36	0.53	0.75	0.43	0.25	0.73	0.43	0.32	0.25	0.50	0.67	0.76	0.24	0.43	0.43	0.19	0.32	0.46
10-13	−5.5	0.18	0.15	0.28	0.14	0.11	0.17	0.26	0.23	0.10	0.20	0.21	0.14	0.09	0.18	0.22	0.28	0.14	0.29	0.29	0.11	0.12	0.19
10-14	−6.0	0.11	0.10	0.14	0.09	0.05	0.10	0.12	0.15	0.04	0.12	0.15	0.14	0.11	0.07	0.12	0.16	0.08	0.13	0.19	0.03	0.08	0.11

[a] Fractional reduction in coolant channel area for individual channels.

[b] Fractional reduction in coolant channel area — average of all channels.

[c] Center line of grid spacer at +3.0 in. position.

[d] Distance from center line of grid spacer.

[e] F_A and $\bar{F}_A$ for sections −3, −4, −5, and −6 calculated from Eq. (6) (F'_A and $\bar{F}'_A$).

[f] F_A and $\bar{F}_A$ for all sections calculated from Eq. (6) (F'_A and $\bar{F}'_A$).

Fig. 11. Posttest View of Test Bundle 1. This photograph shows the deformed area in the first 13-rod transient burst test (300 psig, 95°F/sec). Severely swollen areas and rupture openings are visible at several locations.

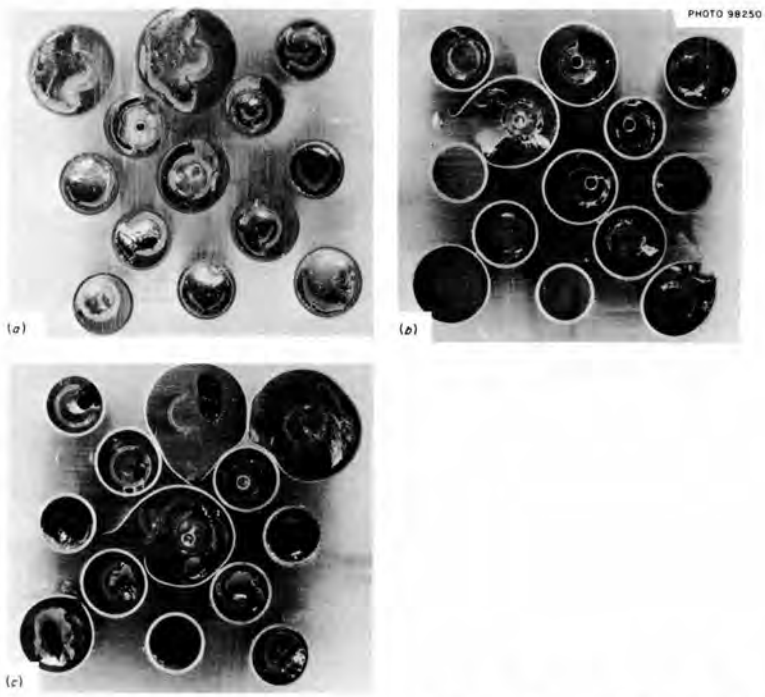

Fig. 12. Cross-Sectional Views of Test 1. The rods in this test were pressurized to 300 psig at 600°F and heated at a measured rate of 95°F/sec. Three of the rods lost pressure and did not deform appreciably or rupture. (a) Section 1-5A at axial center, $\overline{F}_A = 0.28$. (b) Section 1-2B, 3.75 in. below center, $\overline{F}_A = 0.45$. (c) Section 1-3B, 0.50 in. below center, $\overline{F}_A = 0.50$.

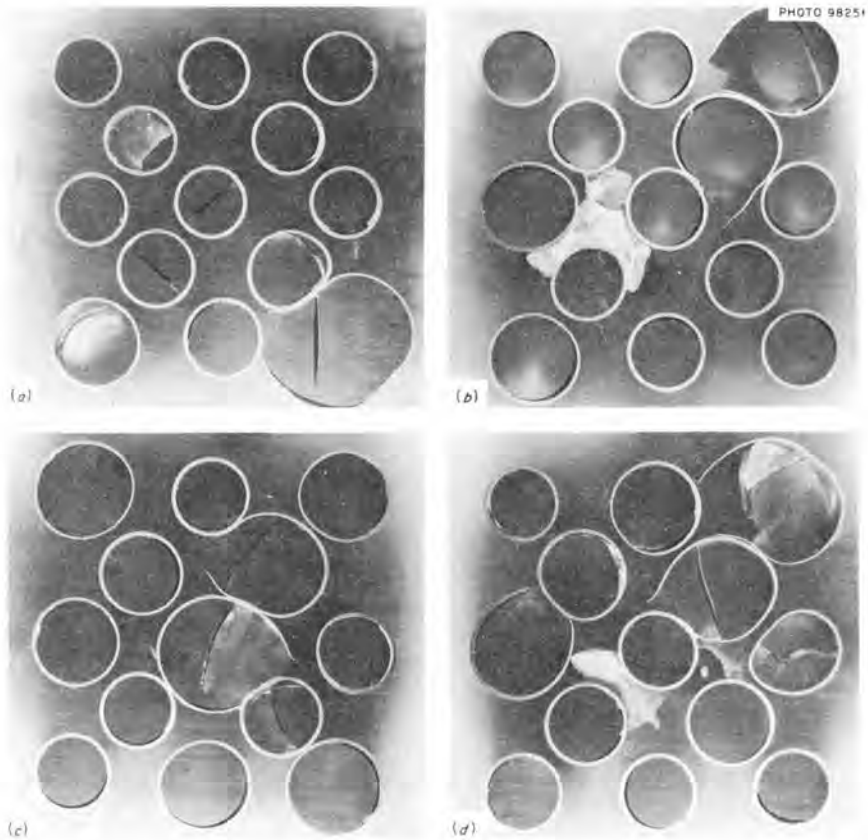

Fig. 13. Cross-Sectional Views of Test 2. Internal pressure in this test was 200 psig at 575°F; heating rate was about 95°F/sec. All rods ruptured. (a) Section 2-3A, 3.15 in. below center, $\overline{F}_A = 0.37$. (b) Section 2-3B, 2.25 in. below center, $\overline{F}_A = 0.47$. (a) Section 2-5B, axial center, $\overline{F}_A = 0.59$. (d) Section 2-5A, 1.5 in. below center, $\overline{F}_A = 0.51$.

as opposed to 1770°F for test 4. Internal pressure at failure was about 425 psig in both tests. All rods ruptured in test 3, but pressure losses resulted in two unfailed rods in test 4. An overall view of the test bundle 4 is given in Fig. 14, and cross sections of the two tests are shown in Figs. 15 and 16.

Test 5 was run at 25°F/sec and 200 psig to failure (all rods) at about 1790°F and 210 psig. Cross sections are shown in Fig. 17.

Test 6 (100 psig, 50°F/sec) was the first in which a grid spacer was used. The grid, at the center of the heated length, resulted in the formation of two distinct deformed regions, each centered about 2 in. from the grid (see Fig. 18). Failure temperature was in excess

Fig. 14. Posttest View of Test Bundle 4. This photograph shows the deformed region in a 400 psig, 25°F/sec test.

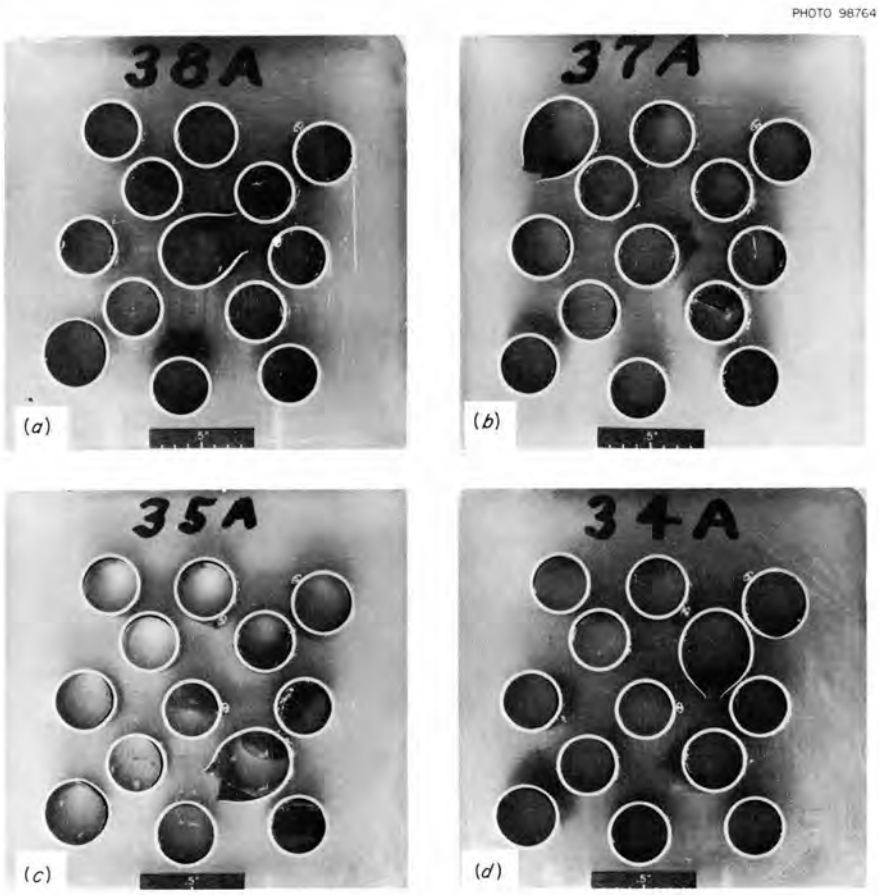

Fig. 15. Cross-Sectional Views of Test 3. All rods ruptured in this 400 psig, 100°F/sec test. (a) Section 3-8A, 1.75 in. above center, $\overline{F}_A$ = 0.21. (b) Section 3-7A, 0.30 in. above center, $\overline{F}_A$ = 0.21. (c) Section 3-5A, 0.75 in. below center, $\overline{F}_A$ = 0.21. (d) Section 3-4A, 1.75 in. below center, $\overline{F}_A$ = 0.21.

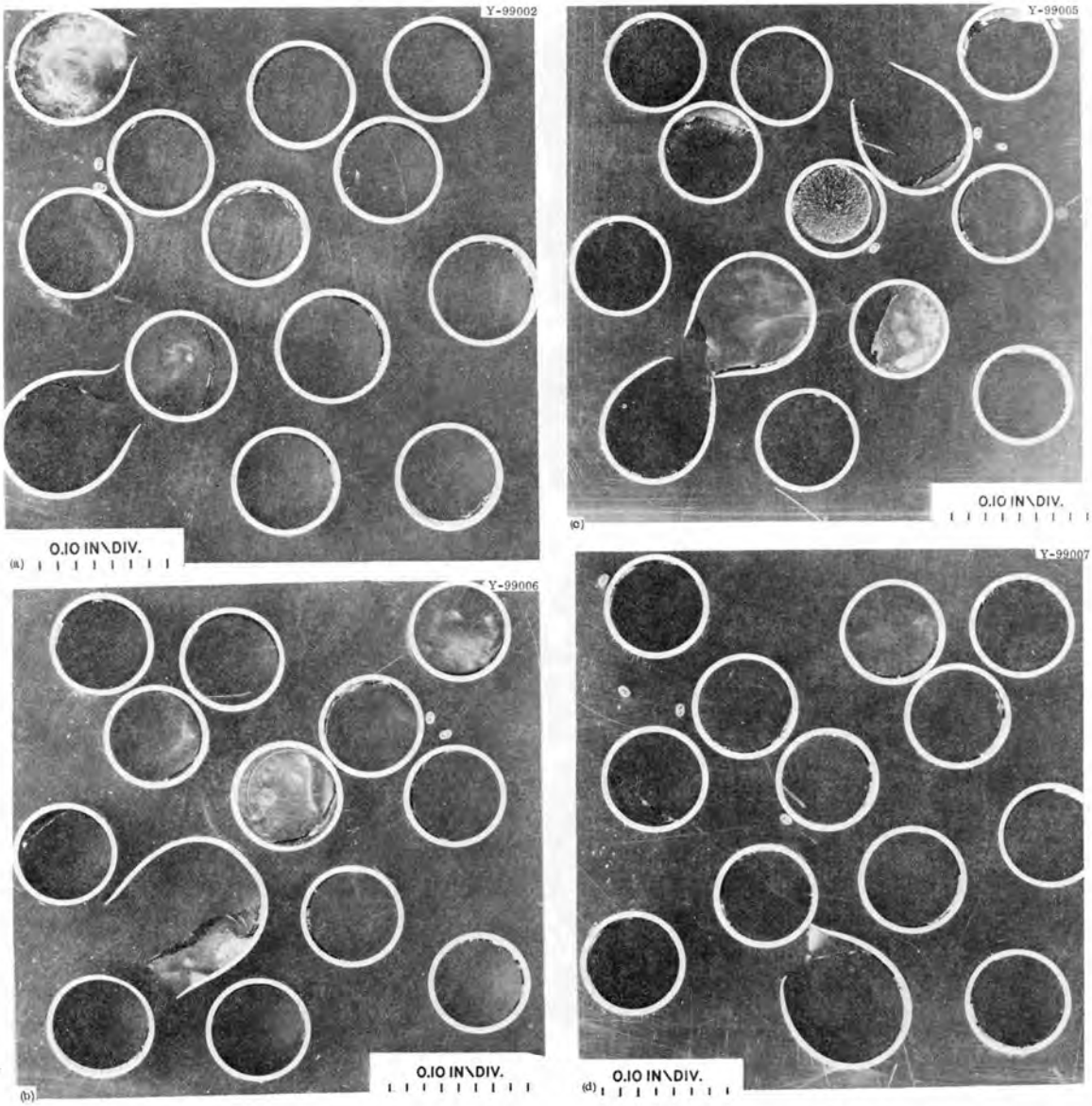

Fig. 16. Cross-Sectional Views of Test 4. In this test, run at 400 psig and 25°F/sec, two of the rods did not rupture. (a) Section 4-3B, 1.25 in. below center, $\overline{F}_A = 0.26$. (b) Section 4-6A, at center, $\overline{F}_A = 0.28$. (c) Section 4-7A, 0.50 in. above center, $\overline{F}_A = 0.28$. (d) Section 4-7B, 2.50 in. above center, $\overline{F}_A = 0.20$.

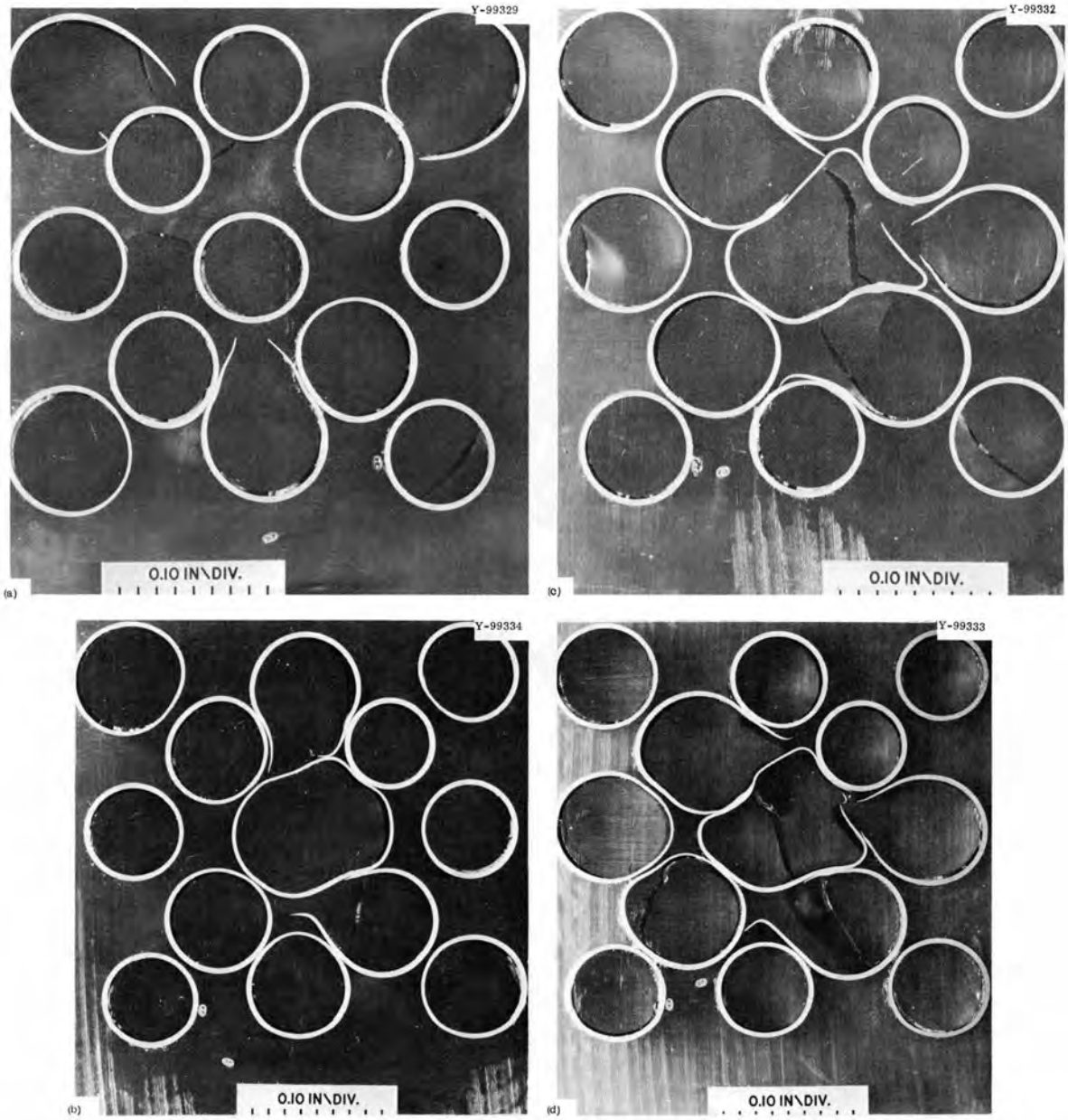

Fig. 17. Cross-Sectional Views of Test 5. This test was run at 200 psig and 25°F/sec. All rods ruptured. (a) Section 5-6A, at center, $\overline{F}_A = 0.27$. (b) Section 5-6B, 0.75 in. above center, $\overline{F}_A = 0.48$. (c) Section 5-7B, 1.25 in. above center, $\overline{F}_A = 0.54$. (d) Section 5-8B, 1.75 in. above center, $\overline{F}_A = 0.56$.

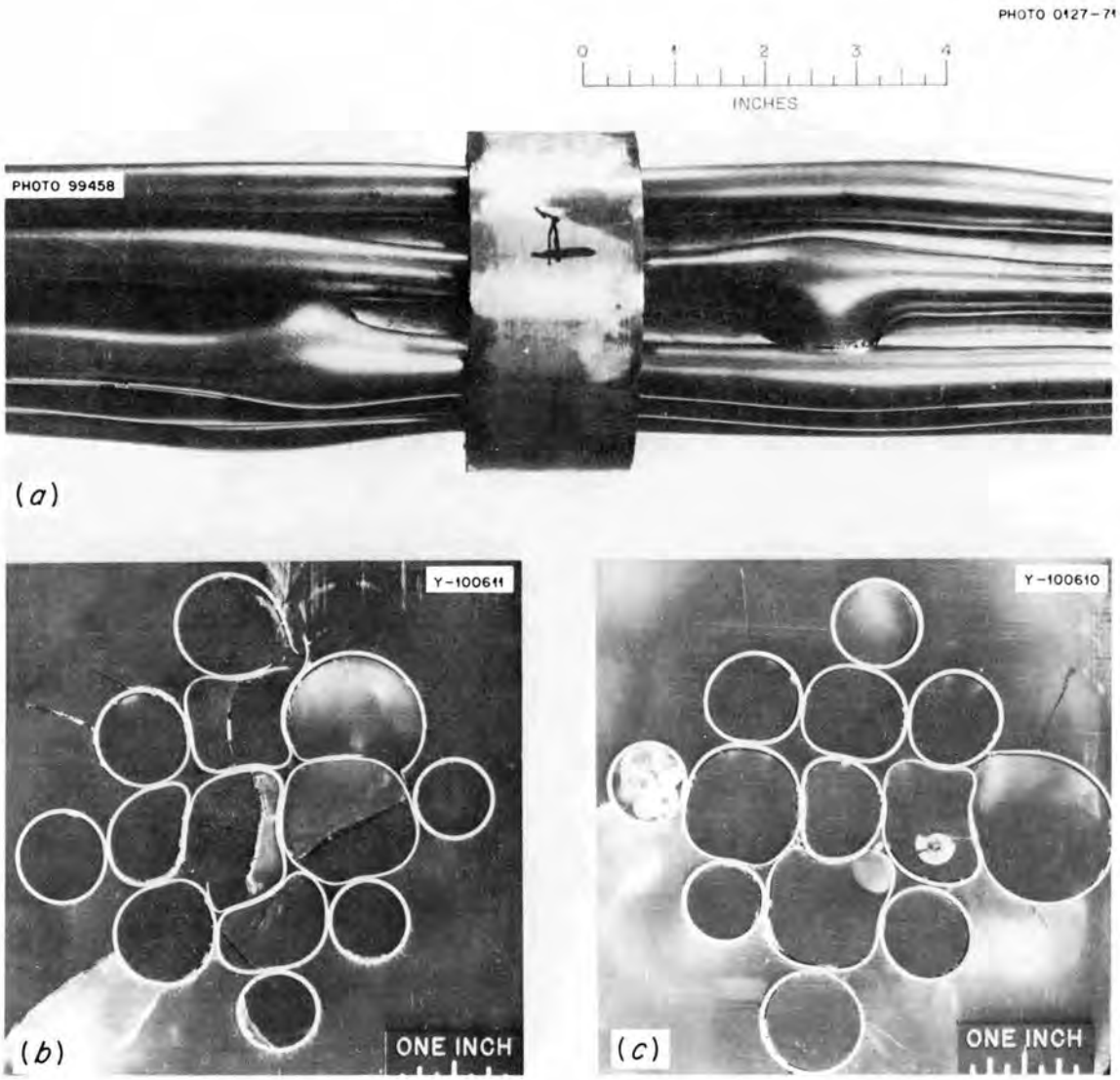

Fig. 18. Posttest Photographs of Test 6. (a) Overall view showing deformed regions and grid spacer. Bundle was pressurized to 100 psig and run at 100°F/sec. Two rods lost pressure and did not rupture. (b) Section 6-2A, 4.40 in. below center, $\overline{F}_A = 0.82$. (c) Section 6-5A, 2.75 in. above center, $\overline{F}_A = 0.76$.

of 2100°F; two rods lost pressure and did not rupture. Two cross sections are shown in Fig. 18.

The first 32-rod experiment successfully completed was test 7. A previous attempt failed because of shorting of the heaters. Test 7 was not without troubles. One of the first rods to rupture destroyed the control thermocouple and resulted in loss of control of the transient

(power to the bundle shut down).[4] Control was manually switched to another thermocouple and the transient was continued until the fuses protecting the power supply SCR's blew. The total time at temperature above 1800°F was sufficient to cause a eutectic reaction between the Zircaloy cladding and the stainless steel grid and subsequent flow of the eutectic downward through the bundle. The rods were extremely embrittled in the region of the grid and it was impossible to mount and section the bundle as in the other tests. Therefore, values of coolant channel blockage were obtained by measuring the diameters of the individual rods at 1/2 in. intervals along their length.

[4]In all tests after test 7, an alternate control thermocouple was installed. This thermocouple would be automatically utilized if the primary thermocouple faulted.

Test 8, as noted in Table 1, p. 12, is being examined by Combustion Engineering.

In test 9, the first of the "high-pressure" tests (700 psig), power was shut off immediately after the four pressure cells indicated cladding rupture. The order of rupture was rod 14 followed by rods 27, 8, and 32. This order is consistent with location within the bundle. When rod 14 ruptured, the temperature on an adjacent rod (TC-1 on rod 13) was 1550°F; the maximum temperature reached was about 1600°F. When the bundle was examined, it was found that only 24 of the rods had ruptured (see Fig. 19). Some of these were heard to

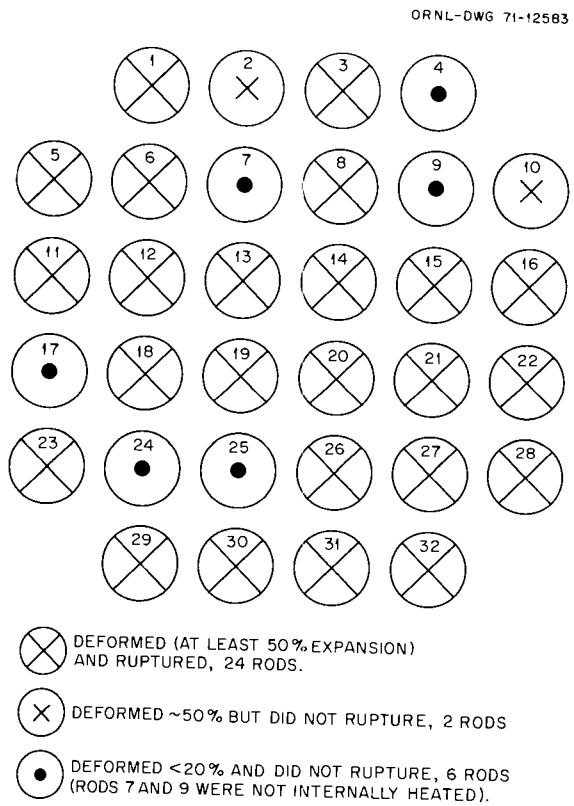

Fig. 19. Deformation and Rupture in Test Bundle 9. This schematic describes the behavior of the individual rods tested at 700 psig, 10°F/sec.

rupture after the power was shut off. Two of the rods, 7 and 9, were intentionally not internally heated. Rods 2 and 10 came very close to failure, and it is likely that only a few additional seconds of power would have resulted in their rupture. Rods 4, 17, 24, and 25 deformed very little, probably because of partial loss of internal pressure. Photographs of the two most highly deformed cross sections are shown in Fig. 20.

Examination of test 10, cross sections of which are shown in Fig. 21, revealed that only half of the rods had ruptured (see Fig. 22) and that nine others had deformed 20 to 50%. The violence of the ruptures forced premature shutoff of the power. It is quite likely, also, that heaters in unfailed rods were damaged by the ejection of gas, lavite, quartz, and tungsten from adjacent rods that ruptured.

Test 11 is being examined by Combustion Engineering.

Coolant Channel Blockage Distribution

Figures 23 through 25 show coolant channel blockage, $\overline{F}_A$, as a function of distance along the test bundle. The data used for the curves are shown in Tables 7 and 8, pp. 18 and 19, respectively. Remember that in test 6 a grid spacer spanned the center 2 in. of the bundle. This accounts for the double peak in the blockage curve (Fig. 24).

As a basis for comparison among the tests, let us consider the length of bundle which experienced blockage of $\overline{F}_A > 0.5$. This is shown in Table 9. In three of the tests (3, 4, and 7), $\overline{F}_A$ was < 0.5 and in the remainder of the tests the length of blockage with $\overline{F}_A > 0.5$ varied from 1 to 6 in.

Figure 26 shows the distance over which the positions of maximum expansion of the tubes occurred in three of the 13-rod tests (tests 2, 4, and 5). The distribution in test 1 was similar to that in test 5 while that in test 6 had two separate peaks. Only in test 3 was the distribution random along the heated length of the bundle. Similar plots are shown in Fig. 27 for the 32-rod experiments. In Fig. 28 we show the number of rods with circumferential expansion in excess of 50% for each axial position.

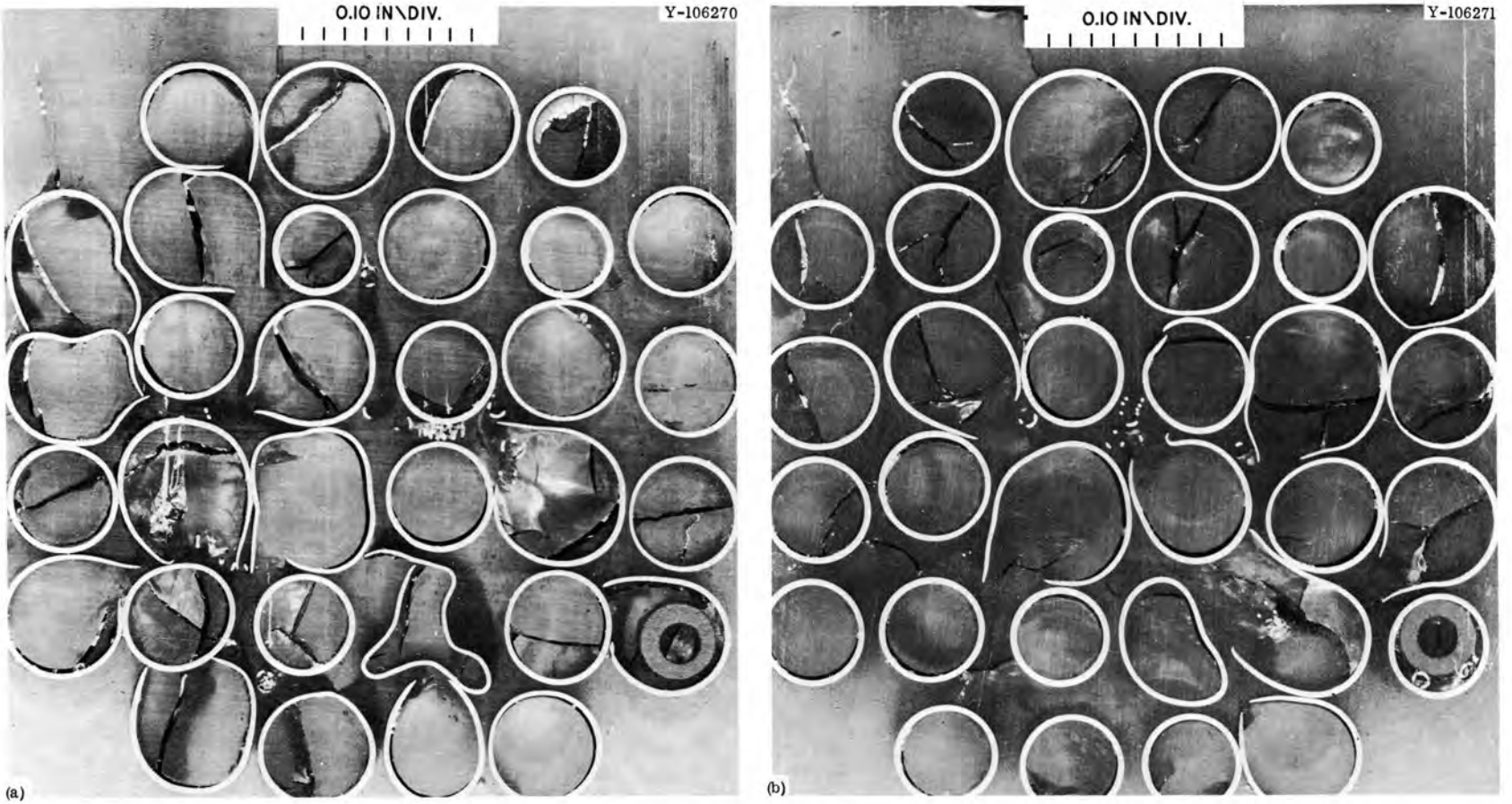

Fig. 20. Cross-Sectional Views of Test 9. In this test, 700 psig and 10°F/sec, 24 of the 32 rods ruptured. (a) Section 9-4, 3.5 in. below the center of the grid, $\overline{F}_A = 0.52$. (a) Section 9-5, 3.0 below center, $\overline{F}'_A = 0.50$.

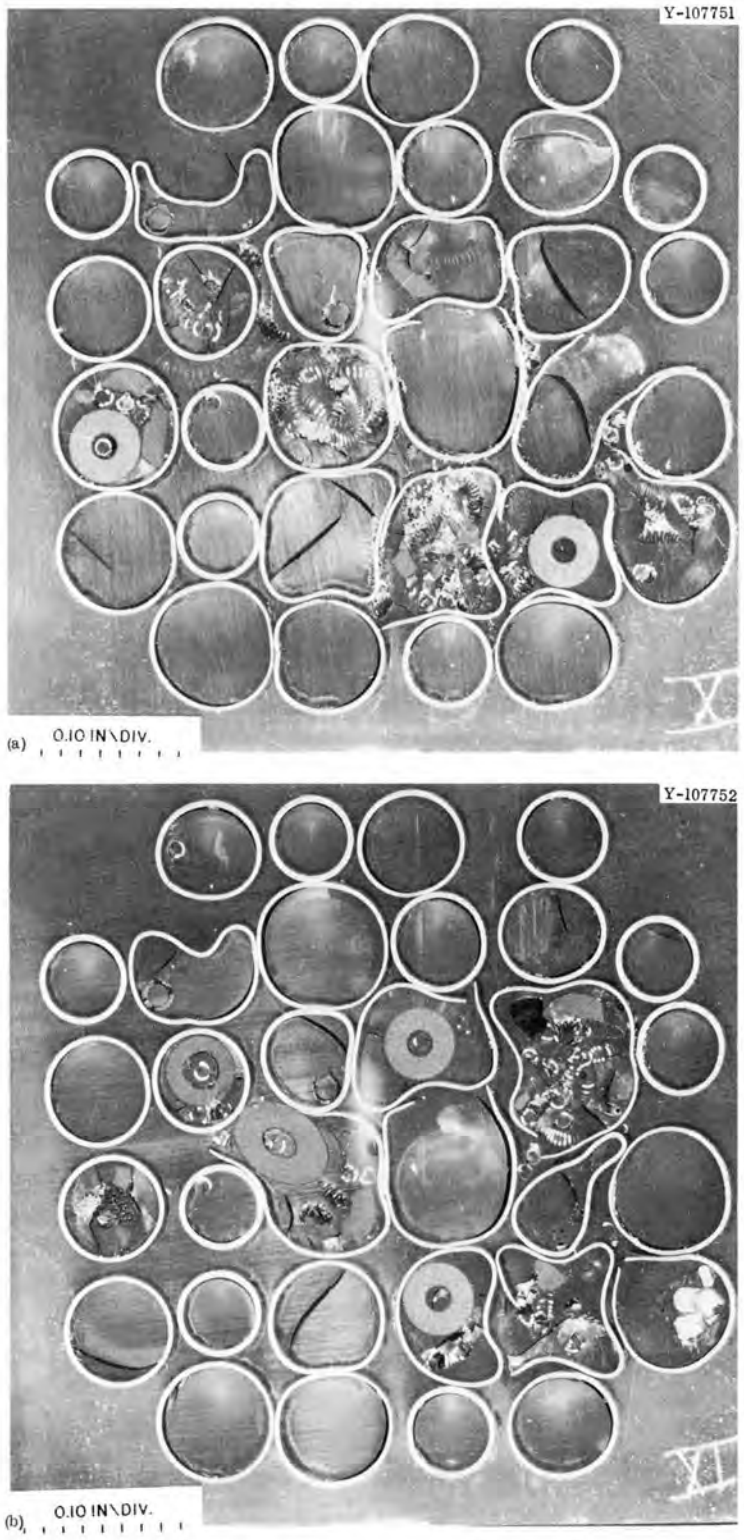

Fig. 21. Cross-Sectional Views of Test 10. Only half of the 32 rods in this 1000 psig, 25°F/sec experiment ruptured. (a) Section 10-10, 4 in. below the center of the grid, $\overline{F}'_A = 0.68$. (b) Section 10-11, 4.5 in. below grid center, $\overline{F}'_A = 0.59$.

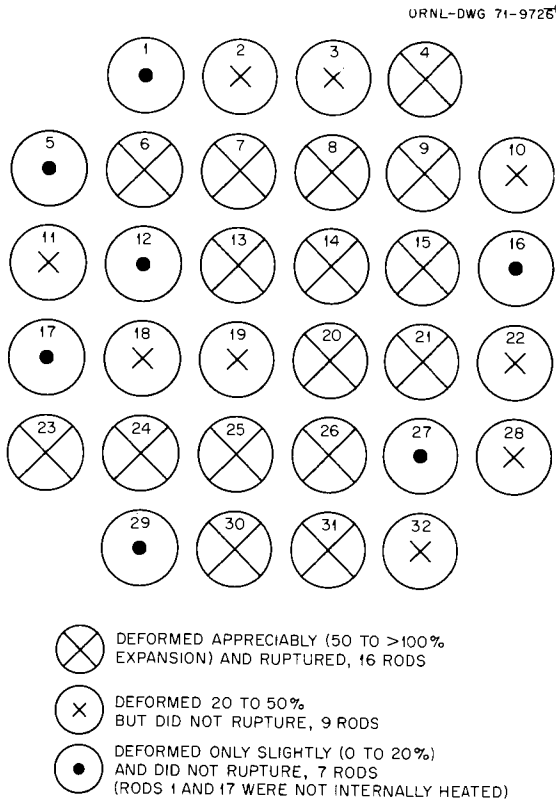

Fig. 22. Deformation and Rupture in Test Bundle 10. This schematic describes the behavior of the individual rods tested at 1000 psig, 25°F/sec.

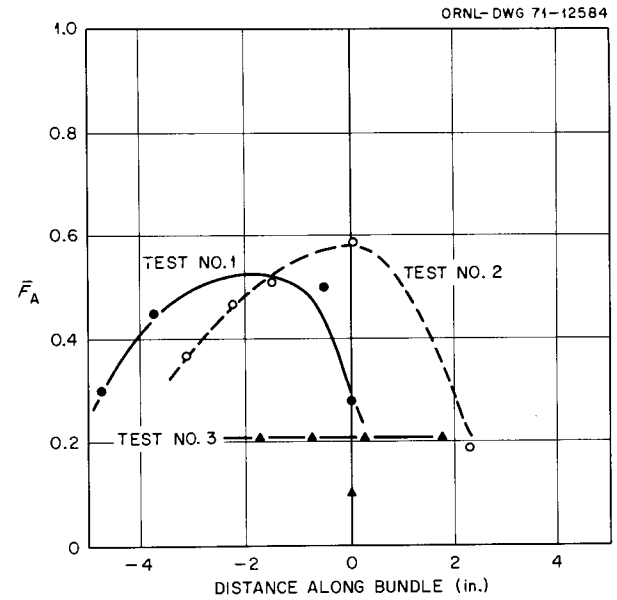

Fig. 23. Coolant Channel Blockage in Tests 1 through 3. Coolant channel blockage, $\bar{F}_A$, is shown as a function of position along the bundle. Distance is given in inches above (+) and below (−) the midpoint or center of the bundle length. Test 1: 300 psig, 100°F/sec. Test 2: 200 psig, 100°F/sec. Test 3: 400 psig, 100°F/sec.

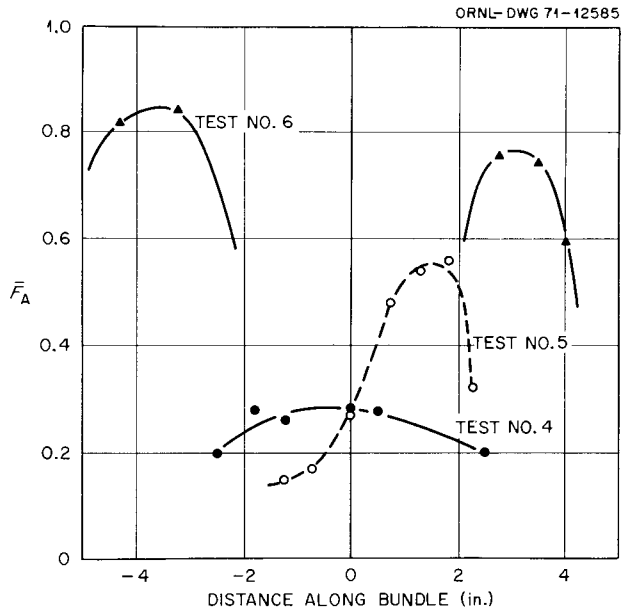

Fig. 24. Coolant Channel Blockage in Tests 4 through 6. $\bar{F}_A$ is shown as a function of position along the test bundle. Test 4: 400 psig, 25°F/sec. Test 5: 200 psig, 25°F/sec. Test 6: 100 psig, 50°F/sec, grid spacer centered at zero position.

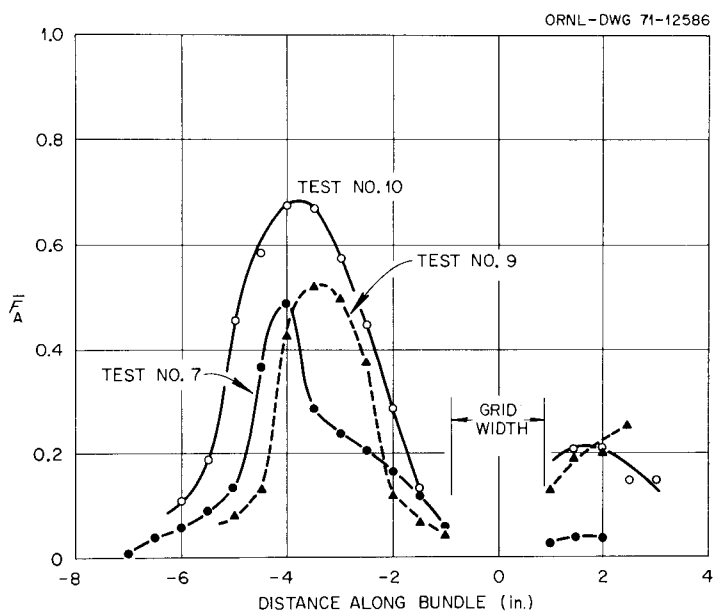

Fig. 25. Coolant Channel Blockage in Tests 7, 9, and 10. $\bar{F}_A$ is shown as a function of distance from the center of the grid spacer. Test 7: 200 psig, 10°F/sec. Test 9: 700 psig, 10°F/sec. Test 10: 1000 psig, 25°F/sec.

Table 9. Comparison of Blockages in the Multirod Tests

Test Number	Bundle Length with $\overline{F}_A > 0.5$ (in.)	Maximum $\overline{F}_A$
1	2	0.50
2	3	0.59
3	0	0.21
4	0	0.28
5	1	0.56
6	6	0.84
7	0	0.49
9	1	0.52
10	2	0.68

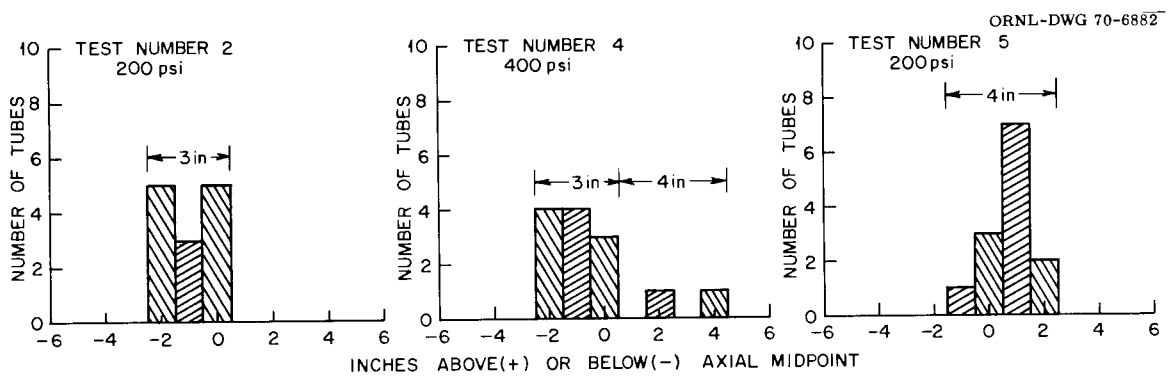

Fig. 26. Histograms of Maximum Deformation. These histograms show the distance over which the positions of maximum expansion of individual rods occurred in tests 2, 4, and 5.

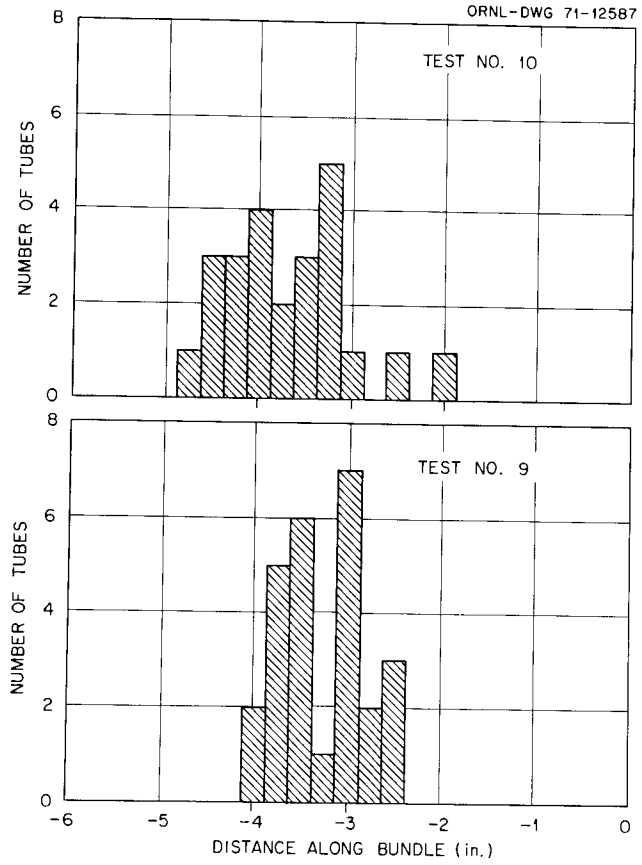

Fig. 27. Maximum Deformation Histograms for Tests 9 and 10. These histograms show the number of tubes that experienced their maximum amount of swelling at a given axial position (the zero position is at the center of the grid spacer). Because some tubes did not deform appreciably, the "number of tubes" does not sum to 32.

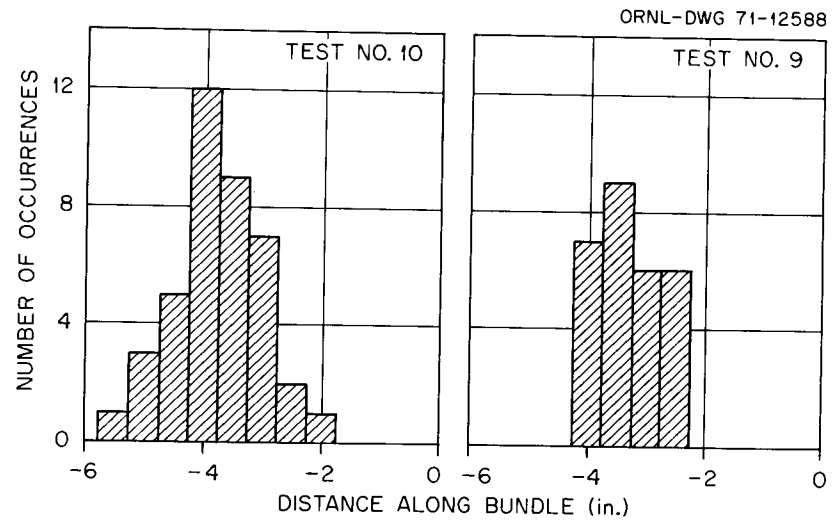

Fig. 28. Fifty Percent Expansion Histograms for Tests 9 and 10. These histograms show, as a function of position, the number of occurrences of swelling or expansion greater than 50%.

DISCUSSION

The Effect of Bundle Size on Test Results

The choice of the bundle size (length and number of rods) used in our multi-tube tests was strongly influenced by equipment availability, performance, and cost. Because the total cost (equipment, material, manpower, etc.) associated with the tests increases in a nonlinear fashion with the number of rods used, it was desirable to hold the bundle size to a minimum. Use of full-length (12-ft) rods was obviously not essential for our purposes. Instead, our tests simulate the hot zone (center 2-ft length) of the fuel rods. Selection of the number of rods in the bundle is not quite so straightforward and, regardless of the number used, it must be possible to extrapolate the results obtained to predict the behavior of fuel rod assemblies. Our analysis of the effect of the number of rods used in a test bundle on the results obtained began with four assumptions: (1) All of the Zircaloy tubes are perfect (i.e., they are of uniform wall thickness and have uniform mechanical properties). (2) Deformation and rupture temperatures are related only to internal pressure and heating rate. (3) The probability that a tube will rupture when any part of that tube reaches the appropriate rupture temperature is unity. (4) All tubes are internally heated with "perfect" heaters (i.e., the radial flow of heat is circumferentially uniform and identical at all positions along the length).

According to the assumptions given above, the position of rupture in a single tube undergoing a thermal transient should be oriented randomly with respect to the circumference of the tube. In a two-tube array the probability for rupture is a maximum, for both tubes, at the point of closest approach of the tubes. (This point is presumably hotter because less heat can be radiated from this point than from any other on the circumference.) The burst characteristics of tubes in larger bundles would be modified similarly. Some examples of this are shown in Fig. 29. The seven different arrays of tubes illustrate, qualitatively, the likelihood for rupture as a function of position on the circumference. In the first four groupings (through four rods), each tube in the array is

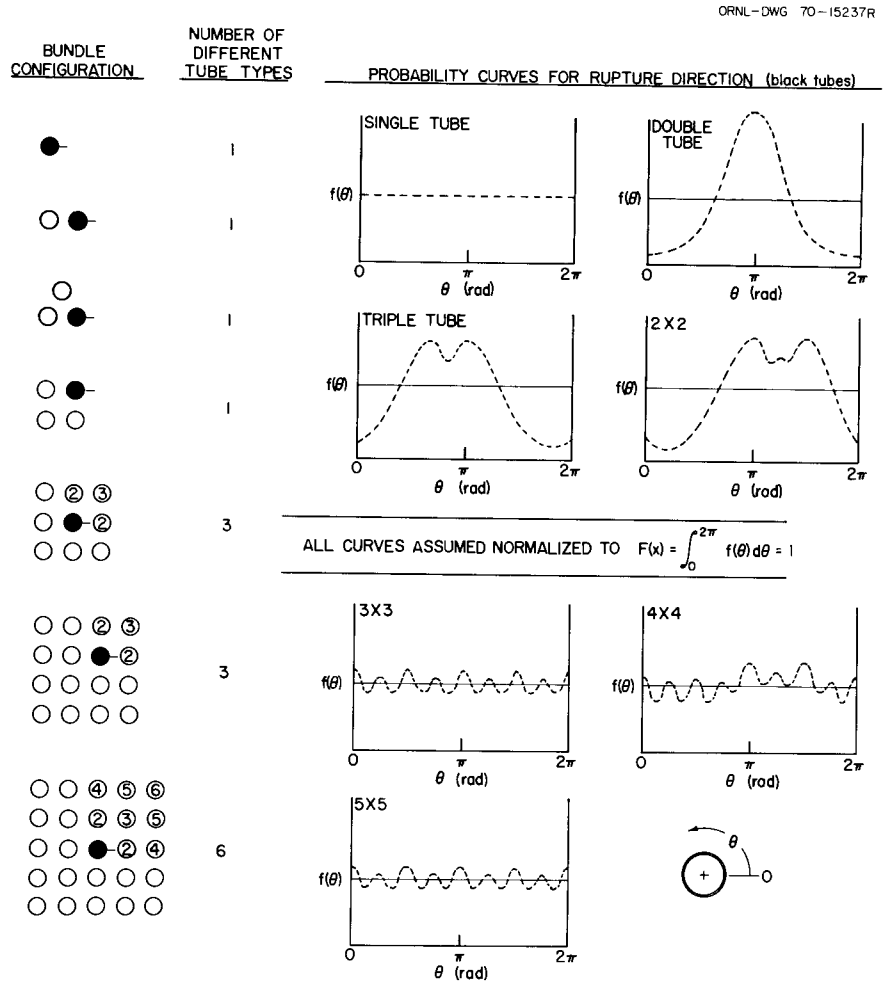

Fig. 29. Bundle Configurations and Directional Rupture Probabilities. Bundles containing 1 to 25 rods are shown. The probability that the rupture opening will be at a particular circumferential position is shown for one rod type (filled) of each array. The probability distribution becomes almost uniform for the innermost tubes of the largest arrays, but not those in the outer rows.

equivalent to its neighbors. The 9- and 16-tube arrays contain three types of tubes (relative to their probability distribution for rupture position) and the 25-tube bundle has six types. The circumferential temperature distribution becomes increasingly complex as more and more tubes are added. In the limit, where a tube is in the middle of an effectively infinite array, its likelihood for rupture is again randomly distributed circumferentially.

From the foregoing it can be postulated that the potential for maximum preburst expansion of a tube can be realized only with a single

tube or with a tube in the center of a large array. (In the latter case the expansion will probably be restrained by interference with adjacent rods.) In every other instance the temperature distribution around the circumference will be nonuniform and plastic deformation will begin and rupture will occur at the hottest point. The strength of the wall at all other lower temperature positions will be greater and deformation, therefore, less. The full potential for swelling will not be realized. Such behavior is analogous to the effect of wall thickness variation on tube expansion[5] (i.e., a tube containing a thin spot in its wall ruptures with less expansion than would a more uniform tube).

Let us consider for a moment the temperature distribution in a 25-tube bundle. With equal power inputs to each rod, the highest temperature will be on the center rod, rod 1, as shown in Fig. 30. The graph on the right of the figure shows, schematically, the temperature history for three rod positions. It is assumed that at high temperature, where radiation is the dominant heat transfer mechanism, the tubes nearer the outside heat up less rapidly than those toward the center of the bundle.

[5]D. O. Hobson and P. L. Rittenhouse, Deformation and Rupture Behavior of Light-Water Reactor Fuel Cladding, ORNL-4727 (September 1971).

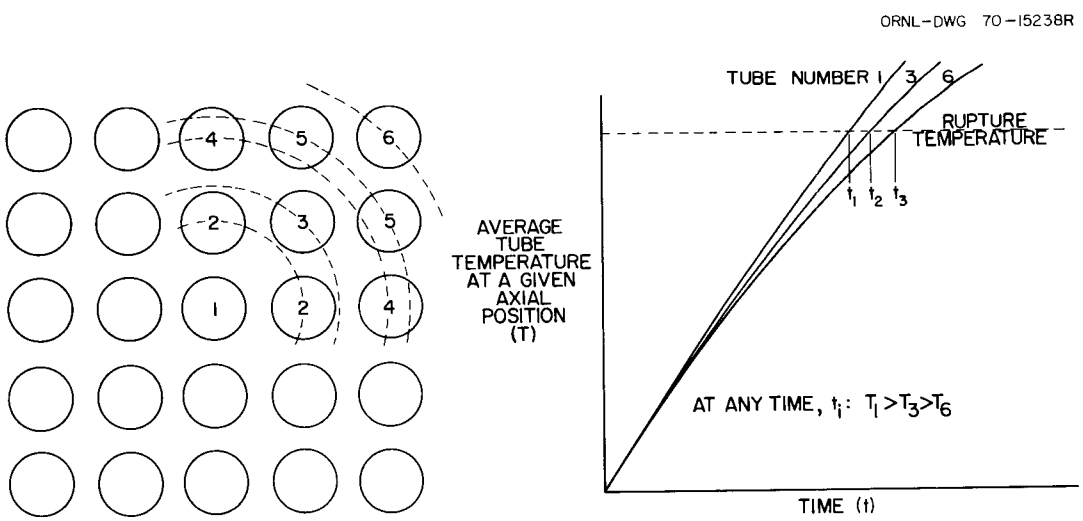

Fig. 30. Radial Temperature Distribution in a 25-Rod Bundle. Equivalent rods in a 5 × 5 array are identified by numbers 1 through 6. Temperature as a function of heating time is shown schematically for three of the rod positions.

Tube 3, as shown in Fig. 31, sees hotter tubes, 1 and 2, on one side and cooler tubes (4, 5, and 6) on the other. The resulting circumferential temperature gradient leads to heat transfer by conduction within the wall of the tube. The magnitude of the gradient should be related to the overall heating rate of the bundle.

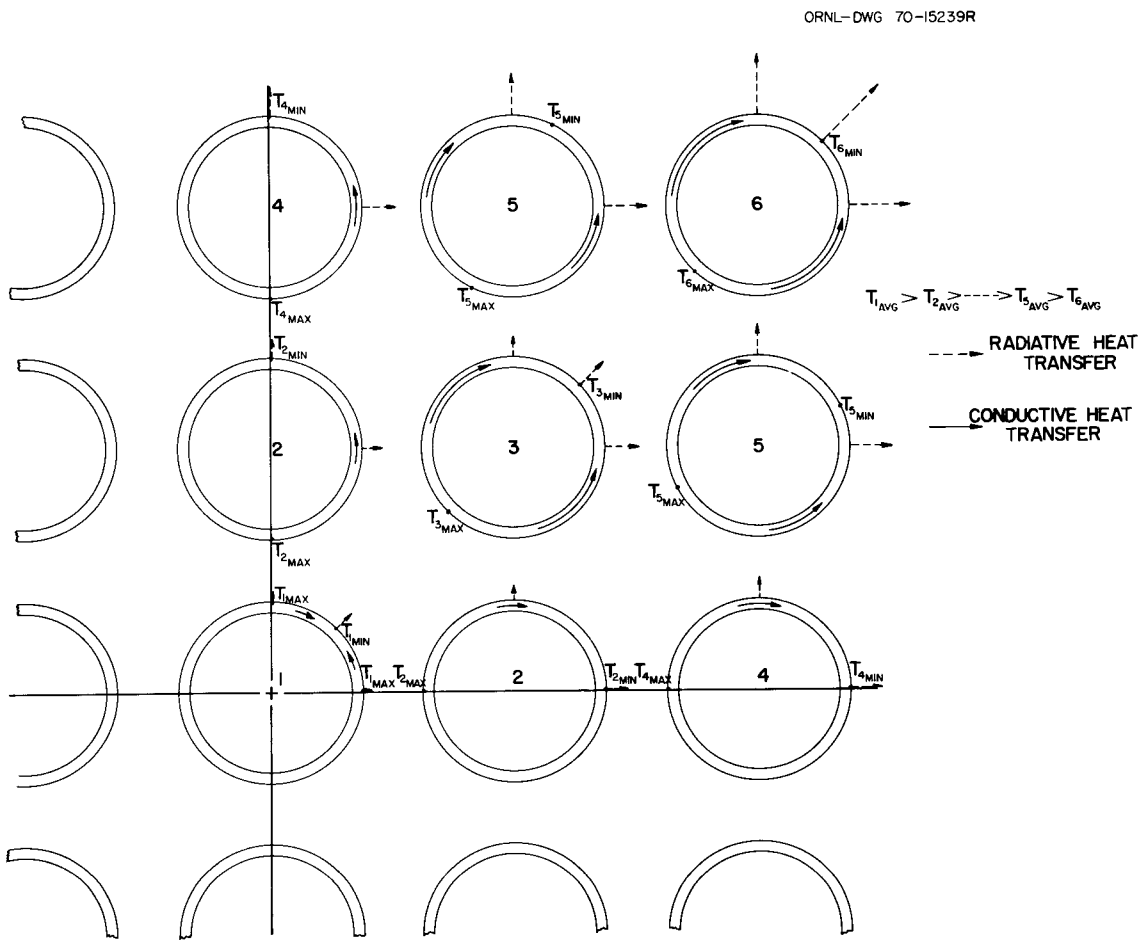

Fig. 31. Radiative and Conductive Heat Transfer in a 5 × 5 Array. Temperatures and heat transfer components in the 25-rod bundle are illustrated. The relative magnitudes of the radiative and conductive components of heat transfer are indicated by the lengths of the appropriate dashed and solid lines, respectively.

In the above we have assumed that the tubes are perfect and will rupture at temperatures related solely to internal pressure and heating rate when any part of the tube reaches the appropriate temperature. At

best these assumptions are approximate. All real tubes are less than perfect, with wall thickness variations, strength variations, flaws, scratches, and other compromising attributes. Also, we know that in all cases the heating of the tubes will be less uniform than assumed. In short, the preceding arguments are complicated by many factors.

Regardless of the shortcomings of our assumptions, analysis and intercomparison of the data obtained in our tests and extrapolation of these data to predict the behavior of fuel assemblies requires some common base. We have attempted to establish this by assigning to each coolant channel a relative measure of applicability or realism with respect to the blockage it should experience. This measure, the channel coefficient (C_c), is dependent only on thermal environment. To specify this coefficient, we first assigned an efficiency to each rod based on its number of nearest and next-nearest neighbors. Each rod in an infinite array of similar rods would possess an efficiency of unity (i.e., there would be no net radiative heat transfer to or from its neighbors). For our purposes we have assumed that a rod with four nearest and four next-nearest neighbors also has an efficiency of unity. This is not strictly true (as evidenced in Fig. 29), but it is a sufficient approximation for a first look at the problem.

We can now define the efficiency of a rod with four nearest and four next-nearest neighbors as

$$\text{Efficiency} \equiv 4w_N + 4w_{NN} \equiv 1.0 \ , \tag{7}$$

where w_N is the contribution of a nearest neighbor rod to efficiency and w_{NN} is that of a next-nearest neighbor rod. To solve this equation for w_N and w_{NN}, we let

$$w_{NN} \equiv w_N\left(d_N/d_{NN}\right) \ , \tag{8}$$

where d_N is the center-to-center distance between nearest neighbor (fuel rod pitch) and d_{NN} is the distance between next-nearest neighbors, $\sqrt{2}d_N$. Solving, we find that $w_N = 0.1465$ and $w_{NN} = 0.1035$. The channel coefficient, C_c, is obtained simply by averaging the efficiencies of the four rods surrounding the channel.

Coefficients for the 21 channels of the 32-rod bundle and the four full and eight half channels of the 13-rod assembly are shown in Fig. 32. In the larger assembly, the coefficients range from 0.76 for the eight corner channels to 1.00 for the centermost channels. Coefficients in the smaller bundle are either 0.79 or 0.41. The bundle coefficient, B_c, is obtained by averaging the channel coefficients.

$$B_c = \sum_{i=1}^{m} C_c/m \ , \tag{9}$$

where m is the number of channels. For the 32-rod bundle

$$B_c = \frac{5(1.00) + 4(0.97) + 4(0.82) + 8(0.76)}{(5 + 4 + 4 + 8)} = 0.87$$

and for the 13-rod test

$$B_c = \frac{4(0.79) + 8/2(0.41)}{(4 + 8/2)} = 0.60.$$

It is interesting to examine the effect of bundle size on B_c. Figure 33 shows this dependence as a function of the number of rods in a square array. B_c increases from 0.40 for the single channel of a 2×2 array to 0.95 for the 196 channels of a 15×15 bundle. For all square arrays larger than 2×2, B_c is given by

$$B_c = [(n - 1)^2 + 4(n - 1)(0.82) + 4(0.68)]/(n + 1)^2 \ . \tag{10}$$

The number of rods in the array is given by $(n + 2)^2$ for $n = 1, 2, \ldots$ and the number of channels is $(n + 1)^2$. In Eq. (10) the first term in brackets, $(n - 1)^2$, is the number of channels with $C_c = 1$, $4(n - 1)$ is the number with $C_c = 0.82$, and the third term shows that there are four corner channels, regardless of bundle size, with $C_c = 0.68$. In all square arrays of size 3×3 or larger, only these three coefficients — $C_c = 1.00$, 0.82, or 0.68 — will be found.

The 7×7 array ($B_c = 0.88$, 16 channels with $C_c = 1$) is of particular interest since this is the size of the BWR fuel bundle. The C_c's

ORNL-DWG 71-1166

BUNDLE COEFFICIENT = 0.87 (21 CHANNELS)

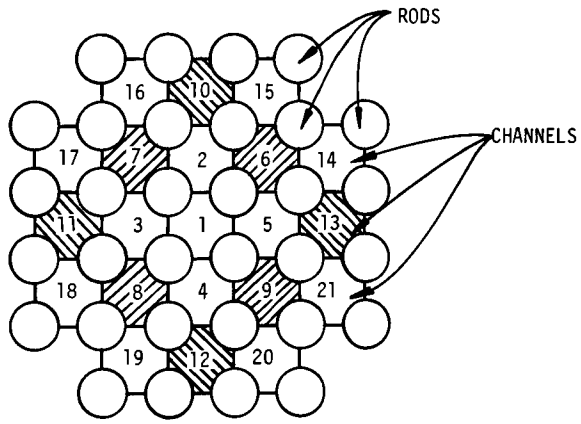

32-ROD EXPERIMENT

CHANNEL NUMBER	CHANNEL COEFFICIENT
1-5	1.00
6-9	0.97
10-13	0.82
14-21	0.76

(a)

ORNL-DWG 71-12589

BUNDLE COEFFICIENT = 0.60

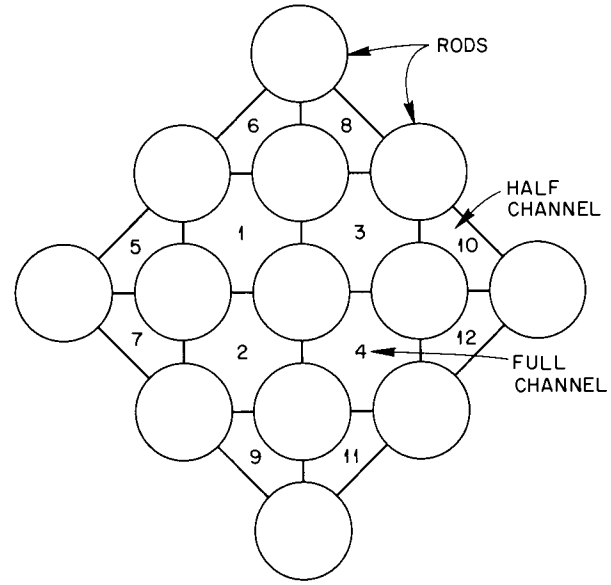

13-ROD EXPERIMENT

CHANNEL NUMBER	CHANNEL COEFFICIENT
1-4 (FULL CHANNELS)	0.79
5-12 (HALF CHANNELS)	0.41

(b)

Fig. 32. Channel Coefficients for the 13- and 32-Rod Arrays. (a) Coefficients, C_c's, for the four types of full channels (1–5, 6–9, 10–13, and 14–21) are shown. (b) C_c's for the four full (1–4) and eight half (5–12) channels are shown.

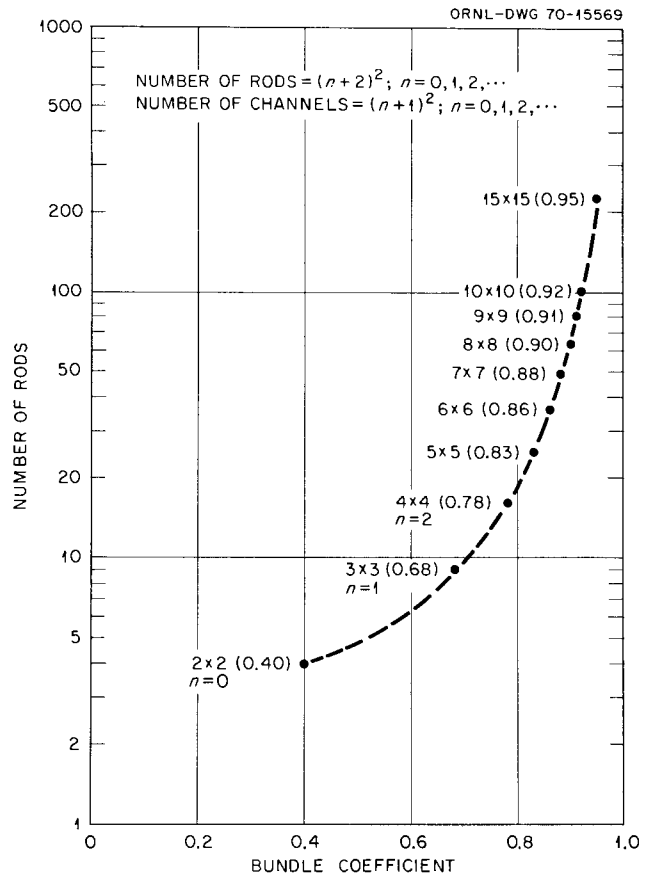

Fig. 33. Effect of Bundle Size on the Bundle Coefficient. The bundle coefficient, B_c, is given as a function of the number of rods in square arrays ranging in size from 2 × 2 to 15 × 15. Increasing the number of rods from 4 to 16 (channels from 1 to 9) doubles B_c; going from 25 to 225 rods (16 to 196) increases B_c by about 15%. $B_c \rightarrow 1$ as the number of rods, $(n + 2)^2$, $\rightarrow \infty$.

for this array are shown in Fig. 34(a). Corner channels have $C_c = 0.68$, side channels have $C_c = 0.82$, and the remainder of the channels have a coefficient of unity. In examining a real fuel bundle, consideration must be given to power peaking in the fuel rods. Figure 35 shows C_c's calculated for two conditions of maximum local power peaking. (All C_c's shown in Fig. 35 are normalized with respect to the highest C_c calculated in the bundle.) The details of the power distributions examined are relatively unimportant for our illustrative purposes because these distributions change continually during reactor power operation. However, in both cases examined the effect was to increase the coefficients of

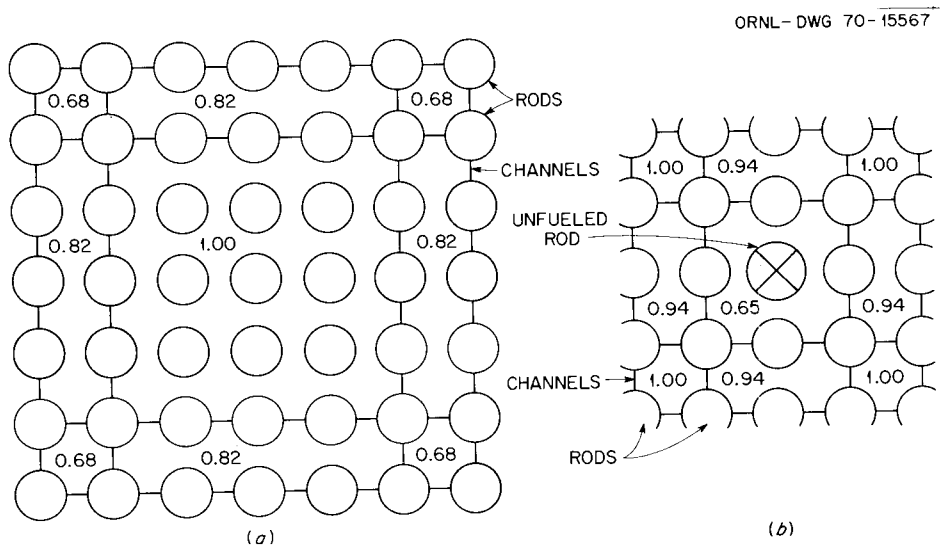

Fig. 34. Fuel Assembly Channel Coefficients (BWR and PWR). (a) The 7 × 7 array of the fuel assembly of a BWR is shown, and the C_c's for the three types of channels are given. C_c's for individual channels will be modified by local power peaking in the rods. (b) The effect of an unfueled rod in a PWR bundle on C_c is illustrated. C_c is significantly reduced, from 1.0 to 0.65 (assuming all C_c's would be 1.0 if all rods were fueled), in the four channels surrounding the rod.

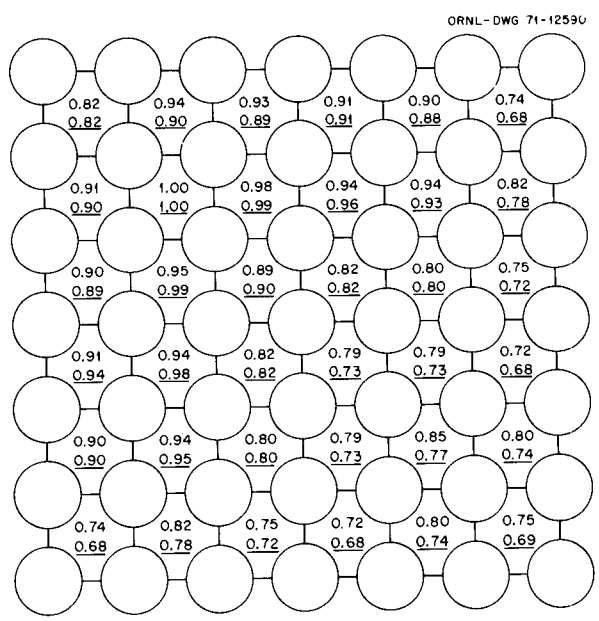

Fig. 35. Modified BWR Fuel Assembly Channel Coefficients. This figure shows individual coefficients, C_c's, calculated for two conditions of maximum local power peaking. One group of C_c's is underlined to differentiate the two conditions. All C_c's are normalized with respect to the highest value of C_c calculated (i.e., maximum calculated C_c normalized to 1.0).

the channels on the left and top of the figure and to reduce those toward the center of the bundle. The B_c's are also slightly changed, falling from 0.88 to 0.85 and 0.83 in the two cases examined, respectively.

The coefficients of channels surrounding an unfueled rod in a PWR fuel bundle were also considered. The coefficients of the four channels immediately surrounding this rod [see Fig. 34(b)] are reduced from 1.0 to 0.65 and those of the next closest eight channels from 1.0 to 0.94. A complete analysis of coefficients throughout the PWR bundle has not been performed but it is expected that C_c's will vary considerably because about 10% of the rods in the 15 × 15 fuel assembly are not fueled.

Relationship Between Coolant Channel Blockage and C_c

If there is any merit to the concept of channel coefficients, we should find that coolant channel blockage, F_A, is a function of C_c and increases as C_c increases. However, we should not expect any such relationship to be unique (i.e., it will be different for every combination of internal pressure and heating rate). The existence of a relationship between F_A and C_c is suggested strongly by data such as shown in Fig. 36 for test 7. Two curves are shown; one is the average of the F_A's for the five center channels (1–5) with $C_c = 1.0$ and the other is for channels 14–21 with $C_c = 0.76$. In the channels with the higher coefficient, the experimentally observed maximum blockage is greater by a factor of 2 and is 50% greater than the maximum average blockage, $\overline{F}_{A_{max}}$.

If we plot an averaged F_A (at axial position of maximum blockage) versus C_c, we obtain the curve shown in Fig. 37. The four values of C_c plotted are those associated with the channel grouping shown earlier in Fig. 32; the F_A's are the averages of those for these groupings – F_A can be represented (as shown in Fig. 37) as $-0.75 + 1.42\ C_c$. At the position of next highest blockage, $F_A = -0.68 + 1.20\ C_c$. As we move further away from the position of maximum $\overline{F}_A$, F_A becomes more and more independent of C_c. (This latter statement is generally true in all the tests examined.)

In examining F_A-C_c relationships in tests 9 and 10, it must be remembered that in each of these experiments two of the 32 rods were

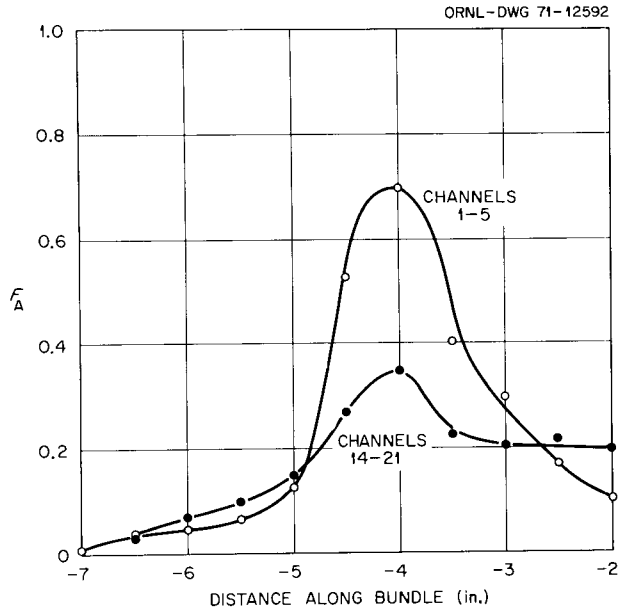

Fig. 36. Coolant Channel Blockage for Two Types of Channels in Test 7. Blockage, F_A, averaged for channels 1 through 5 (C_c = 1.0) and channels 14 through 21 (C_c = 0.76) is shown along the bundle length. At the position of highest blockage, 4 in. below the center of the grid, F_A in the channels of higher coefficient, C_c = 1.0, is twice that in those with C_c = 0.76.

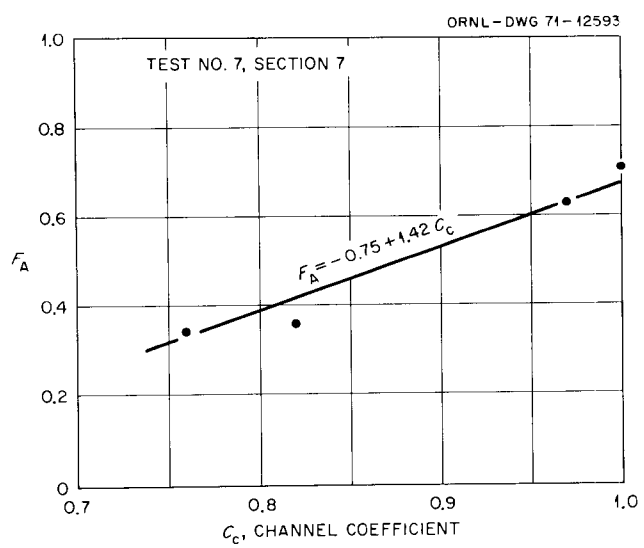

Fig. 37. Variation of Channel Blockage with Channel Coefficients in Test 7. Measured values of blockage (F_A), averaged for each of the four types of channels, are shown as a function of the C_c's associated with these channels. The equation given in the figure is that of the least squares straight-line fit of the data. The blockages shown are those for the cross section with maximum $\overline{F}_A$.

intentionally not heated internally. This, of course, resulted in channel and bundle coefficients different from those in test 7. These modified coefficients are shown in Fig. 38. Grouping of channels was performed to obtain four "average" values of C_c for each test. These values are used in the F_A versus C_c plots that follow.

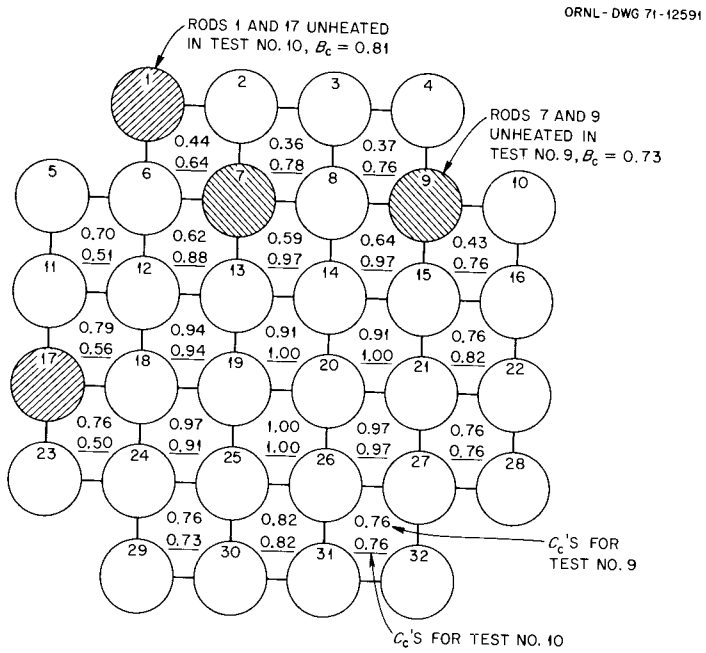

TEST NO. 9

CHANNEL NUMBER	C_c	AVERAGE C_c
1,3,4,5,8,9	0.91 TO 1.00	0.93
11,12,13,18, 19,20,21	0.76 TO 0.82	0.77
2,6,7,17	0.59 TO 0.70	0.64
10,14,15,16	0.36 TO 0.44	0.40

TEST NO. 10

CHANNEL NUMBER	C_c	AVERAGE C_c
1,2,4,5,6,9	0.97 TO 1.00	0.98
3,7,8	0.88 TO 0.94	0.91
10,12,13,14, 15,19,20,21	0.73 TO 0.82	0.77
11,16,17,18	0.50 TO 0.64	0.55

Fig. 38. Channel Coefficients in Tests 9 and 10. In both of these tests two of the 32 rods were not heated. This resulted in modification of many of the channel coefficients as shown in this figure.

Figure 39 shows variation in channel blockage as a function of channel coefficient averaged for the two most highly blocked cross sections in test 9. As in test 7, F_A increases with C_c. The rate of increase, however, is substantially lower.

The F_A versus C_c plots for two cross sections of test 10 are given in Fig. 40. These sections, 10 and 11, had blockages of 0.68 and 0.59, respectively. Two other sections with equally high $\overline{F}_A$'s (8 and 9) showed

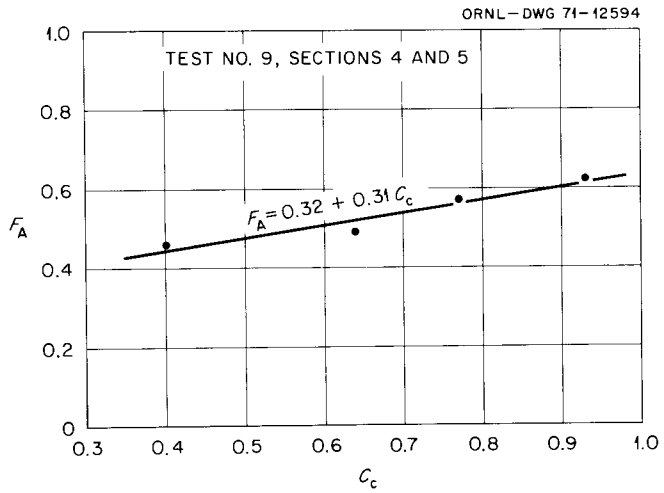

Fig. 39. Variation of Channel Coefficients in Test 9. Blockage data from the two most highly distorted cross sections of test 9 ($\overline{F}_A$ = 0.50 and 0.52, respectively) are plotted versus the appropriate modified channel coefficients given in Fig. 38.

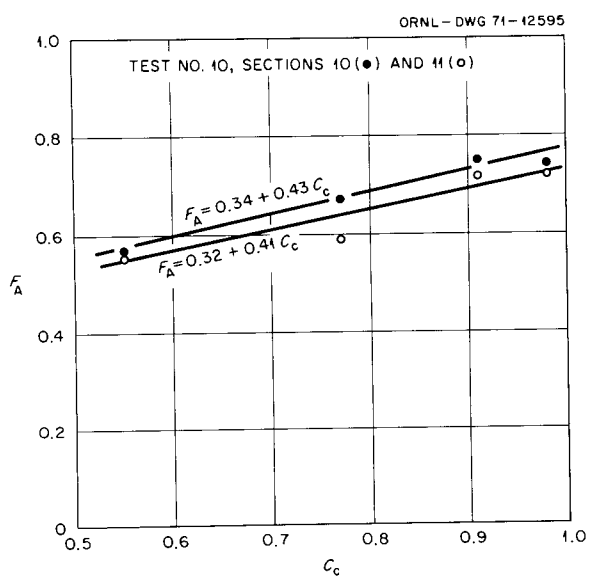

Fig. 40. Variation of Channel Blockage with Channel Coefficients in Test 10. Blockage data from two cross sections of test 10 are shown. Channel coefficients are those shown in Fig. 38.

much more scatter in data and produced F_A versus C_c curves with a slightly negative slope. This is the only instance in which such a trend was observed and, in the cross section just above 8 (section 7), the slope was again positive. We believe that this isolated occurrence is related

to the fact that only half of the rods ruptured and, of the remainder, that seven did not deform appreciably.

In Fig. 41 we show F_A versus C_c plots for all of the 13-rod tests. Although the statistics of these six tests are certainly poorer than those of the three tests with 32 rods (4 full channels and 8 half channels as opposed to 21 full channels), the results seem quite consistent. The magnitude of F_A decreases with internal pressure (from 100 to 400 psig) but its rate of increase with C_c is relatively unaffected by pressures from 100 to 300 psig. Also shown in Fig. 41 are the curves presented earlier for the 32-rod tests. Only in the case of test 7 is there some worry about the consistency of the results. The fact that this test (200 psig, 10°F/sec) yields a lower F_A is not so worrisome (it perhaps fits in the progression with tests 2 and 5) as the large difference in slope of its curve as compared to those of tests 2 and 5. This difference (1) may be real, (2) may reflect a fundamental difference in bundle configuration, (3) may be related to the analysis of

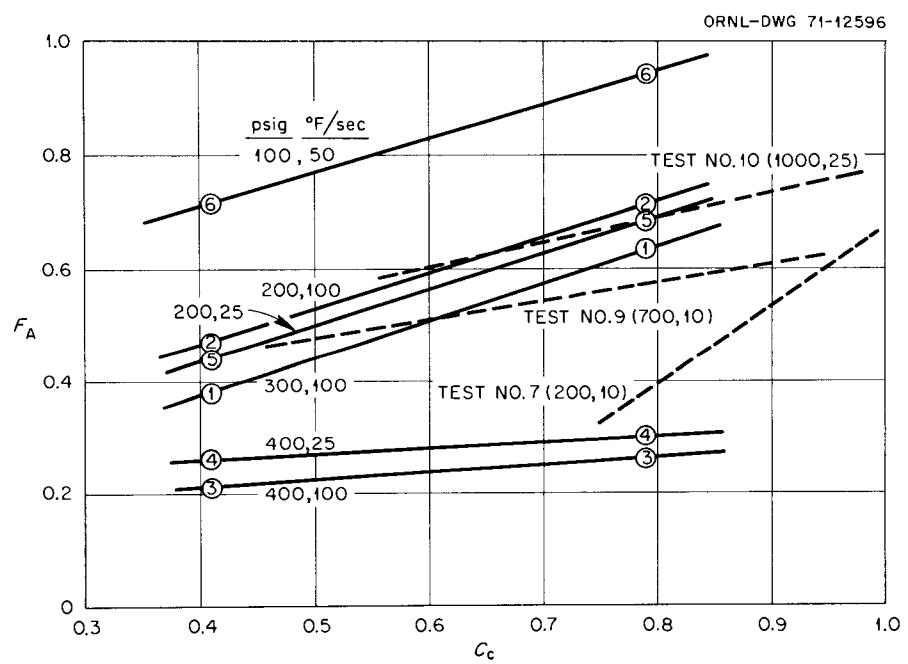

Fig. 41. Variation of Channel Blockage with Channel Coefficients in the 13-Rod Tests. This figure shows the effect of channel coefficients on blockage in tests 1 through 6. Nominal test conditions associated with each test are given. The curves shown previously for the 32-rod tests (7, 9, and 10) are also given to allow comparison of all the data.

half versus full channels, (4) may reflect the restraining influence of the grid spacer used in test 7, but not in tests 2 and 5, or (5) may be related to the difficulties encountered in the experiment and described earlier. None of these possibilities can be totally discounted without further experimental work.

Relationship Between Coolant Channel Blockage and Test Conditions

In the Introduction we predicted coolant channel blockage as a function of maximum internal pressure of the rods during a temperature excursion. The range of F_A or $\overline{F}_A$ predicted is shown again as the cross-hatched region of Fig. 42. The solid curve in the same figure is the representation of our experimentally determined blockages ($\overline{F}_A$). We can see that the form of this curve follows that predicted extremely well but that the magnitude of the experimental blockage, $\overline{F}_A$, is quite a bit lower. This latter observation is not surprising because of the many factors discussed earlier (i.e., axial randomness of position of maximum rod swelling and rupture, rod-to-rod interference, the effect of C_c, etc.). A curve of similar form (the dashed-line curve in Fig. 42) which more closely approaches the predicted range of $\overline{F}_A$ can be obtained by extrapolation of the F_A versus C_c plots (see Fig. 41) to $C_c = 1.0$. This curve, however, still falls on the low side of the predicted range. Some of the remaining difference between experiment and prediction is certainly the result of failure randomness and interference (e.g., at about 400 psig, where failure position was observed to be quite random over the length of uniform temperature, the difference between experiment and prediction is quite large). In other instances, however, the comparison is complicated by the "incompleteness" of failure (i.e., two of the rods in test 6 did not deform and rupture and in tests 7 and 9 a substantial fraction of the rods did not fail). Had "complete" failure occurred both the "experimental" and "extrapolated" curves in Fig. 42 would be higher at the 100 psig and greater than 700 psig regions.

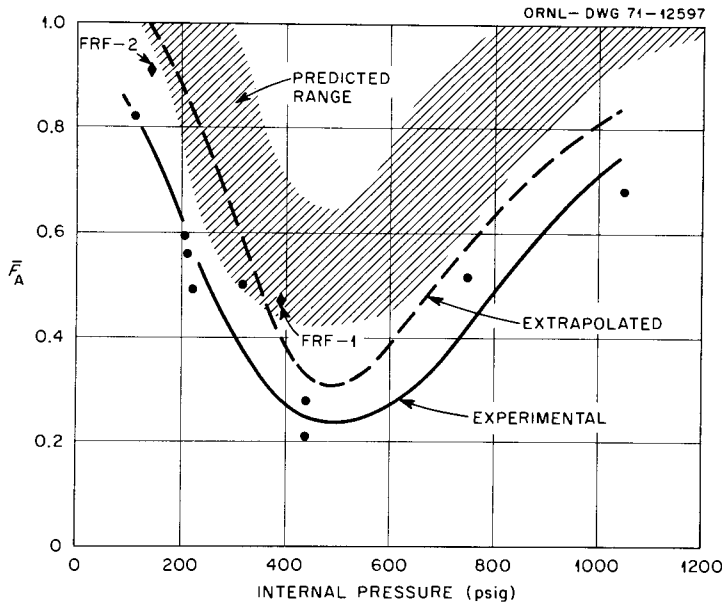

Fig. 42. Comparison of Experimental, Extrapolated, and Predicted Channel Blockages. The average blockage in the most highly blocked cross section, maximum $\bar{F}_A$, is shown as a function of rod internal pressure. The circles, the data points from the multirod tests, define the "experimental" curve; the "extrapolated" curve was obtained by extrapolating F_A versus C_c plots to $C_c = 1.0$. The "predicted range" is that shown earlier in Fig. 2. Data from two in-reactor tests (referenced in text), FRF-1 and -2, are also given.

Two additional bits of information are contained in Fig. 42. These are the data points for experiments FRF-1 and -2 (ref. 6). These 7-rod experiments were run in-reactor under conditions similar to those of the tests we have been discussing. Dissimilarities between the two types of experiments included the use of nuclear heating and a steam environment in the FRF tests. The value of $\bar{F}_A$ obtained in both of the in-reactor tests approximates the lower limit of the predicted range and exceeds that of the out-of-reactor experiments.

Coolant Channel Blockages in Reactor Fuel Assemblies

As noted in the Introduction, the internal fission gas pressure in the vast majority of BWR fuel rods never exceeds about 200 psig and many

[6] R. A. Lorenz, "Fuel Rod Failure Under Loss-of-Coolant Conditions in TREAT," Nucl. Technol. 11(4), 502–520 (August 1971).

of the rods will be at lower pressures. (The details of the pressure distribution will, of course, depend on the operating history of the core.) Cladding temperatures of 1800°F and above are therefore necessary to cause significant swelling deformation and subsequent rupture of the fuel rods. If these temperatures are reached in a 7 × 7 fuel assembly as the result of a LOCA, coolant channel blockages of $\overline{F}_A \geq 0.6$ are to be expected. The distribution of the blockage across the fuel assembly will probably be skewed because of the effect of local power peaking on the coefficients, C_c's, of the individual coolant channels. On the whole, however, the effect of power peaking should be to "randomize" the blockage across the assembly [i.e., the distribution of C_c's is randomized by the existence of power peaking as shown by comparison of Figs. 34(a) and 35.]

It should not be expected that the presence of steam will significantly reduce cladding burst ductility and the resultant $\overline{F}_A$ with internal pressures much above 100 psig. This is witnessed by the results of FRF-2 (see Fig. 42). Steam embrittlement should, however, be a factor at very low internal pressures or with very slow heating rates to maximum transient temperature.

Internal pressures in PWR fuel rods may range from the lowest to twice that of the highest we have considered. Therefore, rupture temperature may be as low as 1000°F. In a practical sense, with prepressurized fuel rods, deformation and rupture of the cladding will probably occur over a range of temperatures from 1000 to 1700°F (400 psig and above internal pressure). This suggests that in lower pressure fuel assemblies $\overline{F}_A$ may be as low as 0.2. However, at pressures much above 400 psig, $\overline{F}_A$ increases quite rapidly. At 1000 psig $\overline{F}_A$ is, as a very unconservative estimate, about 0.7 (see Fig. 42). This value is stated as being unconservative because the only data we have in this pressure range is from test 10 in which only half of the rods ruptured.

As stated earlier and shown in Fig. 34(b), there should be areas of much reduced C_c – and, therefore, of reduced blockage – around unfueled rods in a PWR fuel assembly. About 10% of the rod positions in the 15 × 15 assembly are not occupied by fueled rods and these could serve as focal points for relatively unrestricted emergency coolant flow.

An important but unanswered question is the magnitude of $\overline{F}_A$ at pressures of greater than 1000 to about 2000 psig. The predicted range of $\overline{F}_A$ shown in Fig. 42 (up to 1200 psig) should most certainly turn downward above about 1500 psig because ductility at rupture will decrease with temperature below about 1400°F. However, even with about 2500 psig internal pressure the expected rupture temperature is 1000°F and circumferential expansion should be in the range of 60%. This expansion could produce, theoretically, an $\overline{F}_A$ greater than 0.9.

It is an understatement of considerable magnitude to say that the accurate prediction of coolant channel blockage in a LWR core resulting from a LOCA is difficult. As intimated earlier, the blockage that occurs will depend on:

1. internal fission gas pressure,
2. maximum temperature achieved (i.e., whether the temperature reached is sufficient to result in swelling and rupture of the cladding),
3. fuel assembly geometry (i.e., channel coefficients), and, possibly
4. heating rate.

The first of these, fission gas pressure, depends on other factors such as the period of operation of the fuel assembly, operating conditions, and whether the rods were prepressurized. Internal pressure may vary from rod to rod in an individual assembly as well as across the reactor core. The distribution of pressures will change with operating time, operating conditions, and fuel management.

The maximum temperature reached by the cladding is important because it determines, for any given internal pressure, whether the fuel rods will swell and rupture. It is likely that the maximum temperature will vary across the reactor core and within individual assemblies. The temperature and temperature distribution following the LOCA blowdown will depend on all those factors which influence internal pressure and on the LOCA conditions (e.g., break size, depressurization and coolant loss rate, heat removed during the blowdown period, and ECCS response).

We have considered at some length in the body of this report the effect of channel coefficients on blockage. This, in effect, may be thought of as an additional temperature permutation. Temperature gradients around the circumference of a rod or temperature differences between

adjacent rods should lower, at least locally, the potential for coolant channel blockage. In our analyses we considered only the effect of channel environment (i.e., the number of adjacent rods, whether or not the rods were fueled, and local power peaking), but there are other factors (e.g., fuel shifting and rod bowing) that may have a similar effect on temperature or environment and resultant channel blockage.

Although we believe that heating rate has an effect on blockage we have not, with the limited number of tests run, been able to develop a good, quantitative relationship between the two. Fast heating rates tend to raise the temperature at which swelling begins and rupture occurs. This, of course, could either increase or decrease rupture ductility depending on internal pressure. We know that internal pressures that cause the cladding to rupture at temperatures in the two-phase $\alpha + \beta$ field result in relatively lower ductility.[7] If the internal pressure under consideration, at a given heating rate, causes rupture of the cladding at a temperature toward the upper end of the $\alpha + \beta$ field but still in the ductility trough, increasing the heating rate should result in a higher rupture temperature (in the all β field) and greater cladding ductility and channel blockage. On the other hand, decreasing the heating rate for conditions that give a rupture temperature at the lower end of the $\alpha + \beta$ field should decrease rupture temperature to the all α field and again give rise to greater blockage. For rupture temperatures well away from the $\alpha + \beta$ field (corresponding to internal pressures below 200 psig and above 1000 psig), heating rate should have a considerably smaller effect on ductility and blockage.

An additional complication, one that we have not dealt with in this report, is the effect of irradiation on ductility. In the FRF tests mentioned earlier there seemed to be little or no effect, but in both tests fuel burnup and cladding irradiation levels were very low. Single

---

[7]D. O. Hobson and P. L. Rittenhouse, Deformation and Rupture Behavior of Light-Water Reactor Fuel Cladding, ORNL-4727 (September 1971).

rod tests of cladding with higher irradiation levels[8–11] have shown no gross differences between the behavior of irradiated and unirradiated material. In general, a slight reduction in rupture ductility is noted.

With all factors considered and on the basis of present knowledge, what value should be taken as the maximum coolant channel blockage under specified conditions? First, we must realize that any analysis of blockage must be performed as a function of position in the reactor core. It is perhaps most convenient in a thorough examination to break down the analysis into individual fuel assemblies. Of course, it will not be necessary to look at each of the assemblies but at some number considered representative of the core in terms of power, temperature, age, etc. (i.e., many of the fuel assemblies will be, for all practical purposes, equivalent). For each assembly considered an estimate of internal pressure is required as well as its LOCA temperature history. The blockage results predicted will be modified somewhat by factors mentioned earlier such as "test configuration" and power peaking. (Channel blockage results of a simplified examination of a reactor core are given in the Appendix.)

Most importantly, assuming the temperature attained is sufficiently high to cause cladding swelling and rupture, what should be taken as a conservative, but realistic, maximum blockage for various levels of fission gas pressure in the fuel rods? Referring again to Fig. 42, we can see that an overly conservative estimate of blockage, $\overline{F}_A \geq 0.65$ in all cases, is given by the upper limit of the "predicted range." This, from earlier discussion, would apply for pressures to 2500 psig. As seen in Fig. 42, both the "extrapolated" (F_A extrapolated to $C_c = 1.0$) and "experimental" curves fall, in general, below the lower limit of the

---

[8]D. O. Hobson, M. F. Osborne, and G. W. Parker, "Comparison of Rupture Data from Irradiated Fuel Rods and Unirradiated Cladding," Nucl. Technol. 11(4), 479–490 (August 1971).

[9]E. F. Junke and J. F. White, Physical-Chemical Studies of Clad UO_2 Under Reactor Accident Conditions, GEMP-731 (April 1970).

[10]Performance of Zircaloy-Clad Fuel Rods During a Simulated Loss-of-Coolant Accident: Single Rod Test, Vol. II, WCAP-7379 (September 1969).

[11]M. F. Osborne and G. W. Parker, The Effect of Irradiation on the Failure of Zircaloy-Clad Fuel Rods, ORNL-TM-3626 (January 1972).

predicted range. Even though it is expected that blockage should not, because of other factors discussed earlier, reach the full potential predicted from single rod test data, there were several problems in our experiments that probably resulted in a measured blockage lower than true. At present we suggest that any analysis of blockage be based on no less a conservative estimate than the lower limit of the predicted $\overline{F}_A$ versus internal pressure range.

CONCLUSIONS AND RECOMMENDATIONS

We have performed a series of multi-tube transient burst tests to obtain a sound basis for predicting the coolant channel blockage that would occur in a LWR core should the assumed LOCA be experienced. If the temperature attained in the LOCA transient exceeds the rupture temperature of the Zircaloy fuel cladding under the existing state of stress, the expansion of the fuel rods prior to rupture can be given as a function of the fission gas pressure that produced the given stress. A value of maximum theoretical blockage can, in turn, be calculated from the particular expansion obtained. The tests we have run allow us to specify the amount of blockage, primarily as a function of internal pressure, for pressures ranging from 100 to about 1200 psig. Although we predict blockages for pressures greater than 1200 psig, we acknowledge that the experimental data necessary for such a prediction does not, in reality, exist. Instead, these predictions are based on the general trend of materials behavior as a function of rupture temperature.

A large number of factors, including interference between simultaneously deforming adjacent rods, axial randomness of failure position, and test configuration, have the effect of producing a degree of blockage lower than that calculated. Variations in temperature and internal pressure of the rods in a fuel assembly also complicate the picture, though generally tending to reduce the magnitude of the blockage.

With regard to coolant channel blockage in reactor fuel assemblies, the following can be stated.

1. In BWR assemblies, blockage should be essentially nonexistent if the maximum temperature achieved in the LOCA transient is less than

1800°F. Assemblies in which this temperature is exceeded will have coolant channel blockages, $\overline{F}_A$'s, of 0.6 and above depending on internal pressure, temperature gradients, local power peaking, etc.

2. If only prepressurized PWR fuel assemblies are assumed, deformation and rupture temperatures will be, depending on internal pressure, in the range 1000 to 1700°F. These temperature limits correspond to internal pressures of greater than 2000 psig and about 400 psig, respectively. Blockage, $\overline{F}_A$, will be less than 0.5 for the lowest pressure (400 psig), will increase to about 1.0 at 1200 to 1500 psig, and then decrease to about 0.5 at pressures consistent with the approximately 1000°F rupture temperature.

3. The distribution of $\overline{F}_A$ in the core, regardless of reactor type, will depend on the distributions of internal pressure and temperature in the core. The variation of F_A within a fuel assembly will depend on variations in internal pressure, temperatures and temperature gradients, local power peaking, and proximity to fuel channel walls and unfueled rods.

We strongly urge that further experiments be performed to corroborate the results obtained to date and the criteria that we recommend, based on these results, for analysis of coolant channel blockage in a LWR. As it is obvious that experiments at higher internal pressures are needed, the experimental program should include single rod transient burst tests on PWR-size cladding with internal pressures from 1200 to 2500 psig. These tests (about 20 should be sufficient) would inexpensively and quickly scope the high-pressure burst and deformation behavior of the cladding and permit calculation of a maximum theoretical blockage. Multirod tests of PWR-size cladding should also be run. The test conditions chosen should be based on the single rod test results for pressures up to about 2500 psig. Although our multirod experiments can be modified to eliminate or minimize the problem of "incomplete" failure, the straightforward – but more expensive – approach is to go directly to in-reactor experiments in which the rods are nuclearly driven through a simulated LOCA transient. If experiments of this type prove to be excessively expensive or if consideration of time becomes important, a combination of in- and out-of-reactor tests can be used to advantage.

ACKNOWLEDGMENTS

Many thanks are due Tom Brightwell and Paul Jones for their invaluable services in construction, performance, and taking the data from the multirod tests. We also appreciate the assistance of the Instrumentation and Controls Division, Chester Williams in particular, in instrumentation and data acquisition. Our thanks to M. H. Fontana and J. R. Weir for review of this document, to Jane Morrison for suffering through the original draft, and to Frances Scarboro for setup and typing of the final draft. Finally, we acknowledge many helpful and stimulating discussions with staff members from ORNL, the USAEC, and the commercial nuclear industry.

APPENDIX

Simplified Coolant Channel Blockage Analysis

The three examples that follow are given to show the type of results that may be obtained by examination of coolant channel blockage for specific LOCA conditions. A number of assumptions are made in these examples, both because they simplify the examination and because detailed information is lacking.

First, consider a temperature distribution across a PWR core at a time some 20 sec after initiation of a LOCA. This is given in Fig. A-1 for an approximately 1100 MW(e) PWR. For the "beginning-of-life" condition the "hot spot" temperature on the fuel rods reaches as high as 2150°F at 20 sec. We shall assume that this temperature distribution is symmetrical about the center of the core.

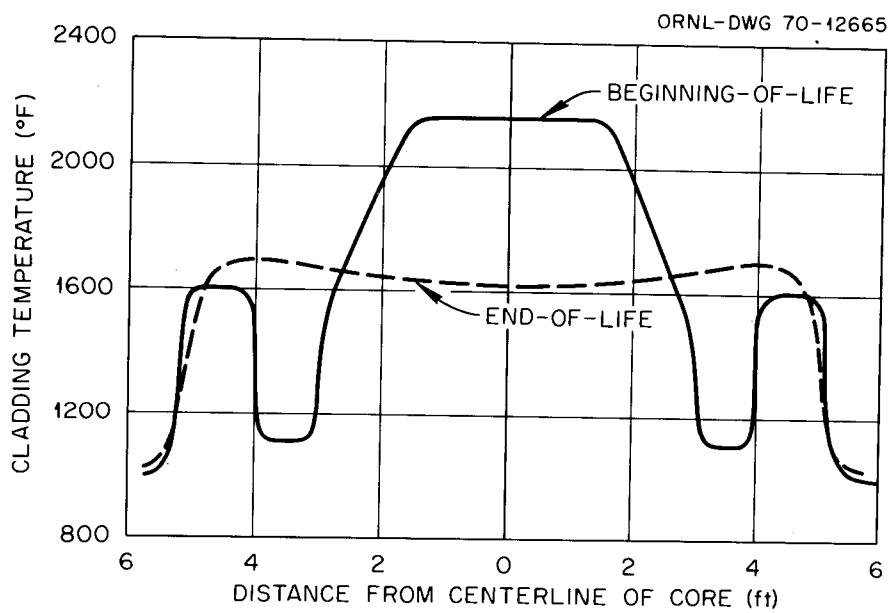

Fig. A-1. Temperature Distribution in a PWR Core Immediately Before Reflooding. The profiles shown are for the midplane of the core 20 sec after a double-ended inlet pipe break in beginning- and end-of-life PWR cores. Profiles were calculated by Idaho Nuclear Corporation. [Ref., J. C. Haire and G. F. Brockett, Technical Description, Simulated Emergency Flow Effects Tests (SEFET) Project, IN-1387 (June 1970).]

Instead of examining individual fuel assemblies, we will divide the core into an arbitrary number of zones. These zones, for our case, are 6-in. radial increments from the core center to its periphery. Thus, zone 1 extends 6 in. in radius from the center of the core; zone 2 extends from the zone 1 boundary to 12 in.; zone 3 is from the zone 2 boundary to 18 in., etc. Each zone has associated with it an average temperature obtained from the "beginning-of-life" curve of Fig. A-1 (see Table A-1).

For example A we assume that the temperatures shown in Table A-1 are the maximum attained during the LOCA. Further, we assume that the internal pressure of fission gases is identical in all rods of the core. Six different levels of internal pressure, from 100 to 1100 psig, are considered. The lower pressures might be representative of the "beginning-of life" core in which the fuel rods are not prepressurized while the higher pressures would be typical of fuel rods prepressurized to various initial levels. The different pressure levels might also be considered as resulting from different operating periods but still early in life.

Fuel rod rupture temperature as a function of internal pressure is shown in Fig. A-2. From this plot we can determine whether the temperature-pressure combination associated with each "core zone" will cause fuel rod deformation and rupture. If rupture is indicated, we can go directly to Fig. 42 (p. 49) and select the coolant channel blockage, $\overline{F}_A$, given by the lower boundary of the "predicted range." If the temperature reached by the zone is less than, but within 50°F of, the rupture temperature, we assume that half of the potential blockage, $\overline{F}_A/2$, is produced. (This is the case for zone 4 at 100 psig in examples A and B of Table A-1.)

Figure A-3 shows coolant channel blockage, $\overline{F}_A$, as a function of distance from the center line of the core. The "data points" are the $\overline{F}_A$'s obtained for each of the core zones. For example, at 100 psig $\overline{F}_A$ for zones 1, 2, and 3 is 1.00, falls to 0.5 for zone 4, and is zero for zones 5 through 12. The potentially most severe blockage is indicated at 1100 psig where, over an area some 6 ft in diameter about the core center (zones 1–6), $\overline{F}_A = 0.95$. The lower temperature, 1150°F, of the

Table A-1. Core Blockage Calculations

Core Zone[a]	Average Temperature[b] (°F)	$\overline{F}_A$																	
		100 psig			300 psig			500 psig			700 psig			900 psig			1100 psig		
		A[c]	B[d]	C[e]	A	B	C	A	B	C	A	B	C	A	B	C	A	B	C
1	2150	1.00	1.00	1.00	0.52	0.52	0.52	0.42	0.42	0.42	0.55	0.55	0.55	0.81	0.81	0.81	0.95	0.95	0.95
2	2150	1.00	1.00	1.00	0.52	0.52	0.52	0.42	0.42	0.42	0.55	0.55	0.55	0.81	0.81	0.81	0.95	0.95	0.95
3	2140	1.00	1.00	1.00	0.52	0.52	0.52	0.42	0.42	0.42	0.55	0.55	0.55	0.81	0.81	0.81	0.95	0.95	0.95
4	2050	0.50	0.50	1.00	0.52	0.53	0.53	0.42	0.43	0.43	0.55	0.52	0.52	0.81	0.76	0.76	0.95	0.92	0.92
5	1850	0	0	0	0.52	0.57	0.57	0.42	0.44	0.44	0.55	0.44	0.44	0.81	0.64	0.64	0.95	0.85	0.85
6	1550	0	0	0	0	0	0	0	0	0.23	0	0	0.42	0.40	0	0.49	0.95	0.34	0.67
7	1150	0	0	0	0	0	0	0	0	0	0	0	0	0	0	0	0	0	0
8	1150	0	0	0	0	0	0	0	0	0	0	0	0	0	0	0	0	0	0
9	1550	0	0	0	0	0	0	0	0	0.23	0	0	0.42	0.40	0	0.49	0.95	0.34	0.67
10	1600	0	0	0	0	0	0.34	0	0	0.45	0.28	0	0.42	0.81	0.25	0.50	0.95	0.70	0.70
11	1175	0	0	0	0	0	0	0	0	0	0	0	0	0	0	0	0	0	0
12	< 1000	0	0	0	0	0	0	0	0	0	0	0	0	0	0	0	0	0	0

[a]Radial increment from center line of core; twelve 6-in. increments.

[b]Average "hot spot" temperature of cladding in "core zone" for calculations A and B. For calculation C, temperature was increased 10%.

[c]In calculation A, the internal pressure of the fuel rods was assumed constant across the core.

[d]In calculation B, internal pressure was assumed to be proportional to the "core zone" temperature [e.g., 100 psig in "zones" 1 and 2 at 2150°F (2610°R); 88 psig in "zone" 5 at 1850°F (2310°R) – 100 psig × 2310°R/2610°R = 88 psig].

[e]In calculation C, the "core zone" temperature was assumed to be 10% greater than shown in column 2. Internal pressure was that used in calculation B.

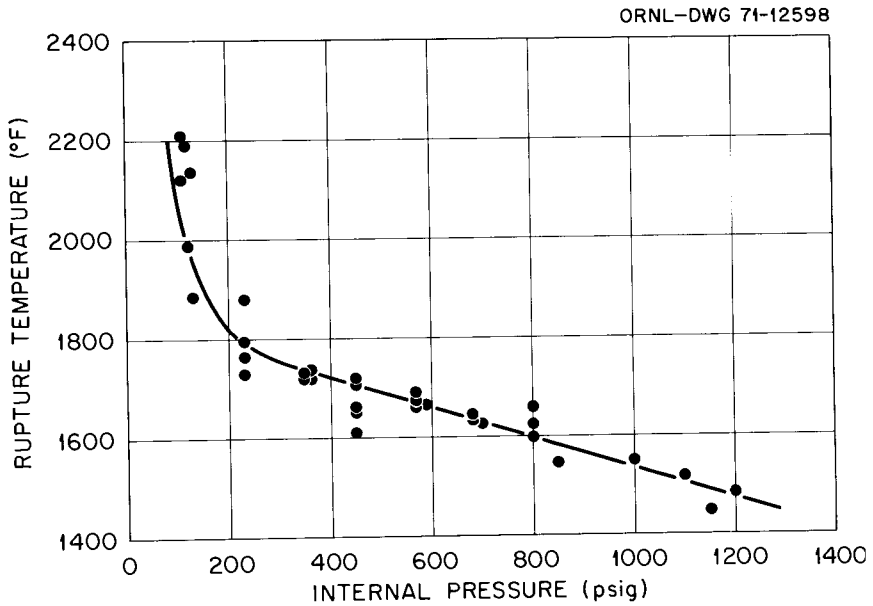

Fig. A-2. Rupture Temperature of Zircaloy Fuel Rod Cladding. This curve gives the rupture temperature of Zircaloy cladding as a function of internal pressure in the fuel rods. The data were obtained in temperature transient burst tests. [Ref., D. O. Hobson and P. L. Rittenhouse, Deformation and Rupture Behavior of Light-Water Reactor Fuel Cladding, ORNL-4727 (September 1971).]

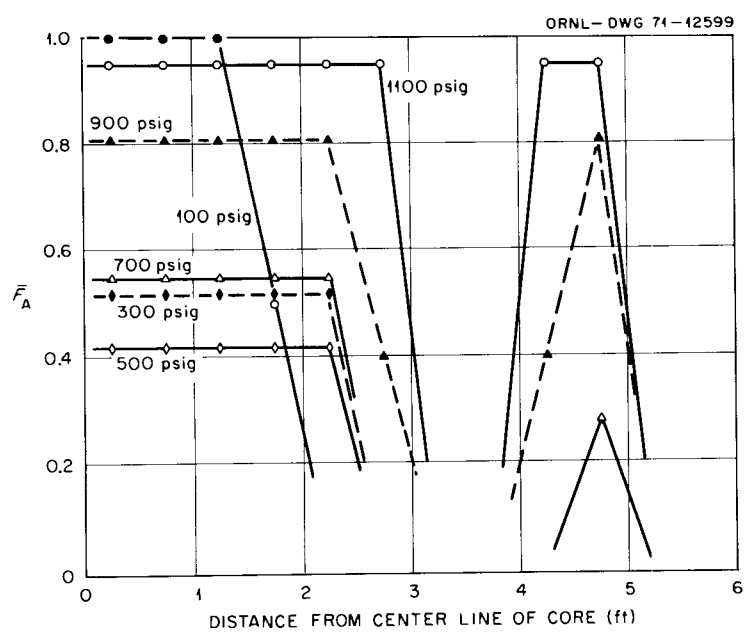

Fig. A-3. Coolant Channel Blockage Across the Reactor Core: Example A. Blockage, $\bar{F}_A$, is shown as a function of distance from the center of the core for six internal pressures (assumed constant core wide) from 100 to 1100 psig. Each data point represents a core zone.

next two zones (7 and 8) is insufficient to cause rupture or significant deformation and $\overline{F}_A$ falls to zero. In the next two zones (9 and 10), however, the temperatures are 1550 and 1600°F, respectively, and rupture can occur ($\overline{F}_A = 0.95$). Based on the total cross-sectional area of the core, only about half experiences this blockage of $\overline{F}_A = 0.95$. However, the portion of the core that is affected is that most in need of emergency cooling water (i.e., the higher temperature portions). Referring again to Fig. A-3, it is seen that both the 100- and 900-psig conditions also produce considerable blockage. Internal pressures of 300, 500, and 700 psig result in blockages expected to be more acceptable in terms of emergency coolant flow and passage.

Example B is given in an attempt to be somewhat more realistic. In this instance it is assumed that the internal pressure of the fuel rods is directly proportional to the maximum, "average hot spot," temperature of the core zone. Therefore, if the pressure is 100 psig in zone 1 (2150°F or 2610°R), it is 100 psig × (2310°R/2610°R) = 88 psig in zone 5, 100 psig × (2010°R/2610°R) = 77 psig in zone 6, etc. This assumption on the proportionality of pressure and temperature has the effect, in general, of reducing the blockage predicted. At 300 and 500 psig, however, $\overline{F}_A$ in zones 4 and 5 is increased slightly (see Table A-1 and Fig. A-4).

Finally, it is interesting to note the effect of increasing the zone temperature. In this case, example C, we have assumed that the temperature of each of the zones is increased by 10% over that shown in Table A-1. Internal pressures assumed are those used in example B. Figure A-5 shows that the higher temperatures assumed result in, when compared with example B, higher blockages but, with a few exceptions, not so high as given in example A. (Zones 1, 2, and 3 show identical results for all the examples.)

A similar exercise can be performed for the "end-of-life" condition. Figure A-1 shows that the temperatures at this stage are much reduced and more uniform across the core. However, internal pressures would certainly be in the range 2000 psig and above, and it is probable that all rods except those at the periphery of the core (zone 12) would rupture. It is likely, then, that $\overline{F}_A$ would be 0.5 to 0.6 all through the core.

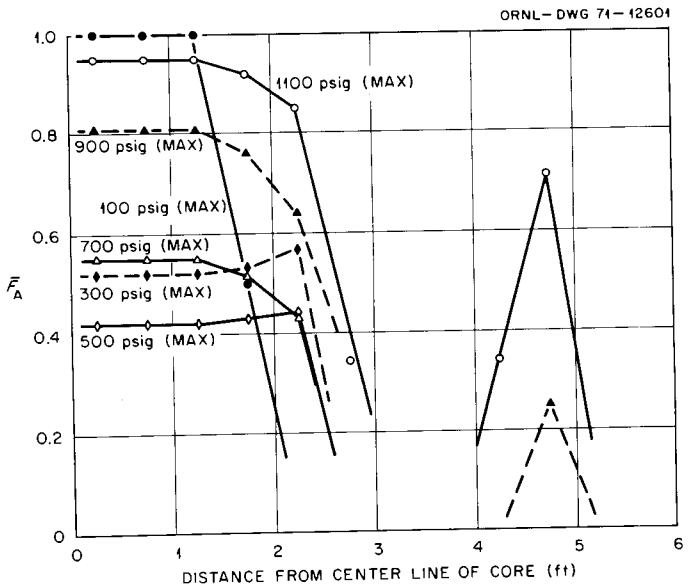

Fig. A-4. Coolant Channel Blockage Across the Reactor Core: Example B. Blockage, $\bar{F}_A$, is shown as a function of distance from the center of the core for six conditions of internal pressure. The internal pressures indicated as maximum are those for the highest temperature core zone. The pressure in other zones is proportional to the temperature.

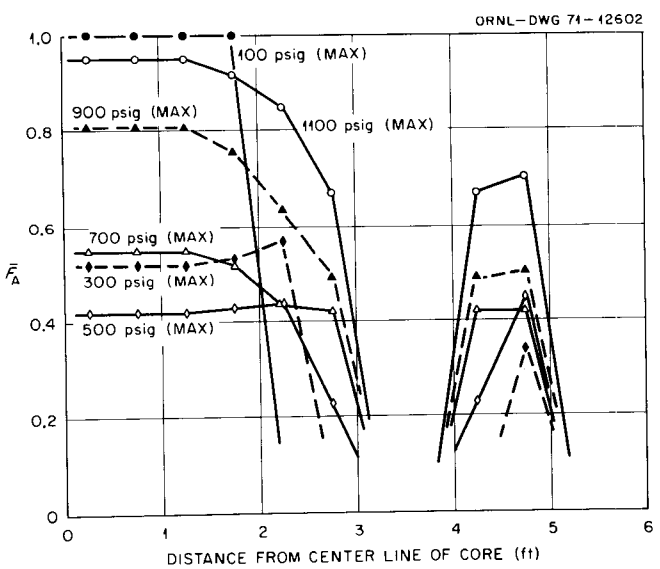

Fig. A-5. Coolant Channel Blockage Across the Reactor Core: Example C. Example C is as B except that the temperatures of the various core zones are increased by 10%.

The examples that have been shown are not intended to represent the situation in any specific reactor, reactor type, or any particular LOCA. Many simplifying assumptions were made in this analysis; details of pressure and temperature distributions need to be considered in an analysis of the "real" situation. However, our examples do demonstrate the effects of pressure and temperature on blockage and give approximations of the blockage conditions that may be experienced should a LOCA occur.

ORNL-4752
UC-80 — Reactor Technology

INTERNAL DISTRIBUTION

1–3. Central Research Library
4. ORNL — Y-12 Technical Library
Document Reference Section
5–25. Laboratory Records Department
26. Laboratory Records, ORNL RC
27. ORNL Patent Office
28. Nuclear Safety Information Center
29. G. M. Adamson, Jr.
30. S. E. Beall
31. R. Blanco
32. R. H. Bryan
33–36. W. B. Cottrell
37. F. L. Culler, Jr.
38. J. E. Cunningham
39. D. Ferguson
40. M. H. Fontana
41. J. H Frye, Jr.
42. W. R. Gambill
43. W. O. Harms
44–46. M. R. Hill
47. R. F. Hibbs
48–57. D. O. Hobson
58. C. G. Lawson
59. R. A. Lorenz
60. A. L. Lotts
61. H. E. McCoy
62. C. J. McHargue
63. M. F. Osborne
64. P. Patriarca
65–74. P. L. Rittenhouse
75. D. B. Trauger
76. R. D. Waddell
77. A. M. Weinberg
78. J. R. Weir, Jr.
79. G. D. Whitman
80. C. M. Adams (Consultant)
81. P. Cohen (Consultant)
82. J. Corbett (Consultant)
83. H. H. Kellogg (Consultant)
84. W. Kohn (Consultant)
85. S. Siegel (Consultant)
86. L. N. Zumwalt (Consultant)

EXTERNAL DISTRIBUTION

87. H. L. Arnold, AEC, Division of Reactor Development and Technology, Washington, DC 20545
88. C. V. Backlund, AEC, San Francisco Operations Office, 2111 Bancroft Way, Berkeley, CA 94704
89. R. H. Ball, Gulf General Atomic, P.O. Box 608, San Diego, CA 92112
90. H. W. Behrman, AEC, RDT, OSR, Oak Ridge National Laboratory
91–92. C. W. Bills, AEC, Idaho Operations Office, P.O. Box 2108, Idaho Falls, ID 83401
93. B. E. Bingham, Babcock & Wilcox Company, P.O. Box 1260, Lynchburg, VA 24505
94. R. G. Bock, General Electric Company, 175 Curtner Avenue, San Jose, CA 95125
95–96. J. F. Boland, TREAT, Argonne National Laboratory, Idaho Falls, ID 83401
97. M. Bolotsky, AEC, Division of Reactor Standards, Washington, DC 20545
98. A. P. Bray, General Electric Company, 175 Curtner Avenue, San Jose, CA 95125
99. J. M. Brett, Babcock & Wilcox Company, P.O. Box 1260, Lynchburg, VA 24505
100–102. G. O. Bright, WRSPO, Aerojet Nuclear Corporation, P.O. Box 1845, Idaho Falls, ID 83401

103. G. Brockett, Aerojet Nuclear Corporation, P.O. Box 1845, Idaho Falls, ID 83401
104–105. R. S. Brodsky, AEC, Naval Reactors Branch, Division of Naval Reactors, Washington, DC 20545
106. G. M. Brown, Southern Nuclear Engineering, P.O. Box 10, Dunedin, FL 33528
107. G. Burley, AEC, Division of Reactor Licensing, Washington, DC 20545
108. S. H. Bush, ACRS, WADCO Corporation, P.O. Box 1970, Richland, WA 99352
109–110. W. A. Carbiener, Battelle Memorial Institute, 505 King Avenue, Columbus, OH 43201
111. M. W. Carbon, University of Wisconsin, Engineering Research Building, Madison, WI 53706
112–122. E. G. Case, Director, Division of Reactor Standards, AEC, Washington, DC 20545
123. J. O. Cermak, Westinghouse Electric Corporation, P.O. Box 355, Pittsburgh, PA 15230
124–125. W. P. Chernock, Combustion Engineering, Inc., 1000 Prospect Hill Road, Windsor, CT 06095
126. J. M. Clabby, Power Authority of the State of New York, New York, NY 10000
127. F. J. Climent, Aerojet General Corporation, Sacramento, CA 95801
128. J. C. Cochran, LMEC, Atomics International, P.O. Box 309, Canoga Park, CA 91304
129. R. J. Colmar, AEC, Division of Reactor Licensing, Washington, DC 20545
130. D. F. Cope, AEC, RDT, SSR, Oak Ridge National Laboratory
131. J. W. Crawford, AEC, Division of Reactor Development and Technology, Washington, DC 20545
132. G. W. Cunningham, AEC, Division of Reactor Development and Technology, Washington, DC 20545
133–134. P. R. Davis, Aerojet Nuclear Corporation, P.O. Box 1845, Idaho Falls, ID 83401
135–136. E. H. Davidson, AEC, Division of Reactor Development and Technology, Washington, DC 20545
137. R. A. Dean, United Nuclear Corporation, Grasslands Road, Elmsford, NY 10523
138. L. Devell, AB Atomenergi, Stockholm, Sweden
139. C. Dickerman, Argonne National Laboratory, 9700 S. Cass Avenue, Argonne, IL 60439
140. Director, Argonne National Laboratory, 9700 S. Cass Avenue, Argonne, IL 60439
141. Director, Brookhaven National Laboratory, 29 Cornell Avenue, Upton, Long Island, NY 11973
142. H. A. Dopchie, Association Vincotte, Rhode-Saint-Genese-Belgium
143. A. R. Duffy, Battelle Memorial Institute, 505 King Avenue, Columbus, OH 43201
144. R. Dunham, Tennessee Valley Authority, Knoxville, TN 37900
145. A. D. Emery, Combustion Engineering, Inc., 1000 Prospect Hill Road, Windsor, CT 06095

146. H. Etherington, ACRS, Jupiter, FL 33458
147. Dieter Ewers, AEG, Telefunkin, E313, 6 Frankfort/Main 70, AEC, Hochhaus Siid, Germany
148. H. K. Fauske, Argonne National Laboratory, 9700 S. Cass Avenue, Argonne, IL 60439
149. Horst Feuerstein, Kernsforschungszentrum, Karlsruhe, Germany
150. John Field, General Electric Company, 310 DeGuigne Drive, Sunnyvale, CA 94086
151. G. Fischer, Argonne National Laboratory, 9700 S. Cass Avenue, Argonne, IL 60439
152. S. Fistedis, Argonne National Laboratory, 9700 S. Cass Avenue, Argonne, IL 60439
153–154. P. Fox, Westinghouse Electric Corporation, P.O. Box 158, Madison, PA 15663
155. D. Fletcher, Westinghouse Electric Corporation, P.O. Box 355, Pittsburgh, PA 15230
156. J. W. Flora, Division of Compliance, Region IV, 10395 W. Colfar Avenue, Denver, CO 80215
157–159. R. F. Fraley, Executive Secretary, Advisory Committee on Reactor Safeguards, AEC, Washington, DC 20545
160. D. M. Gardiner, AEC, Chicago Operations Office, 9700 S. Cass Avenue, Argonne, IL 60439
161. P. Gast, LMFBR Program Office, Argonne National Laboratory, 9700 S. Cass Avenue, Argonne, IL 60439
162. H. Gilbert, AEC, Division of Operational Safety, Washington, DC 20545
163–164. A. J. Goodjohn, Gulf General Atomic, P.O. Box 608, San Diego, CA 92112
165. H. Graves, Westinghouse Electric Corporation, P.O. Box 355, Pittsburgh, PA 15230
166. J. E. Grund, Portland General Electric Company, Portland, OR 97200
167. J. C. Haire, Aerojet Nuclear Corporation, P.O. Box 1845, Idaho Falls, ID 83401
168. G. Hake, Atomic Energy of Canada, Ltd., Chalk River, Ontario, Canada
169. H. L. Hamester, AEC, Division of Reactor Development and Technology, Washington, DC 20545
170. S. H. Hanauer, AEC-REG, Washington, DC 20545
171. Harvard Air Cleaning Laboratory, Harvard University, 665 Huntington Avenue, Boston, MA 02190
172. F. M. Heck, Westinghouse Electric Corporation, P.O. Box 355, Pittsburgh, PA 15230
173. J. E. Hench, General Electric Company, 175 Curtner Avenue, San Jose, CA 95125
174. J. M. Hendrie, ACRS, AEC, Brookhaven National Laboratory, 29 Cornell Avenue, Upton, Long Island, NY 11973
175. K. Hikido, General Electric Company, 310 DeGuigne Drive, Sunnyvale, CA 94086
176. H. M. Hill, ACRS, AEC, Excelsior, MN 55331
177. J. Hillary, Reactor Development Laboratory, Sellafield, Seascale, Cumberland, England

178. A. B. Holt, AEC, Division of Reactor Standards, Washington, DC 20545
179. T. Iltis, Westinghouse Electric Corporation, P.O. Box 158, Madison, PA 15663
180–181. D. H. Imhoff, General Electric Company, 175 Curtner Avenue, San Jose, CA 95125
182–183. R. J. Impara, AEC, Division of Reactor Development and Technology, Washington, DC 20545
184. J. E. Irvin, Battelle Northwest Laboratory, P.O. Box 999, Richland, WA 99352
185. H. S. Isbin, ACRS, University of Minnesota, Minneapolis, MN 55455
186. R. O. Ivins, Argonne National Laboratory, 9700 S. Cass Avenue, Argonne, IL 60439
187. M. E. Jackson, Argonne National Laboratory, 9700 S. Cass Avenue, Argonne, IL 60439
188. H. A. Johnson, University of California, Institute of Engineering Research, Berkeley, CA 94704
189. S. O. Johnson, Aerojet Nuclear Corporation, P.O. Box 1845, Idaho Falls, ID 83401
190. Sigvard Junkrans, Aktibolaget ASEA-ATOM, Västerås, Sweden
191. W. J. Kaufman, ACRS, University of California, Richmond, CA 94804
192. Reese Kern, Aerojet Nuclear Corporation, P.O. Box 1845, Idaho Falls, ID 83401
193. E. E. Kintner, AEC, Division of Reactor Development and Technology, Washington, DC 20545
194. L. Kornblith, Jr., AEC, Division of Compliance, Washington, DC 20545
195. R. E. Kosiba, AEC, Division of Reactor Development and Technology, Washington, DC 20545
196. B. Lamar, Argonne National Laboratory, 9700 S. Cass Avenue, Argonne, IL 60439
197. T. W. Laughlin, Chief, Document Management Branch, Division of Technical Information Extension, Oak Ridge, TN 37830
198. W. H. Layman, AEC, Division of Reactor Development and Technology, Washington, DC 20545
199. M. C. Leverett, General Electric Company, 175 Curtner Avenue, San Jose, CA 95125
200. J. V. Levy, General Electric Company, 310 DeGuigne Drive, Sunnyvale, CA 94086
201. A. Lohmeier, Westinghouse Electric Corporation, Heat Transfer Division, Lester Branch Box 8175, Philadelphia, PA 19113
202. A. Lowe, Babcock & Wilcox Company, P.O. Box 1260, Lynchburg, VA 24505
203. J. Lytton, Virginia Polytechnic Institute, Department of Metallurgical Engineering, Blacksburg, VA 24061
204. Manager, Chicago Operations Office, AEC, 9700 S. Cass Avenue, Argonne, IL 60439
205. Manager, Idaho Operations Office, AEC, P.O. Box 2108, Idaho Falls, ID 83401
206. Manager, Oak Ridge Operations Office, AEC, Oak Ridge, TN 37830
207. Manager, New York Operations Office, AEC, 376 Hudson Street, New York, NY 10014

208. Manager, Richland Operations Office, AEC, P.O. Box 500, Richland, WA 99352

209. Manager, San Francisco Operations Office, AEC, 2111 Bancroft Way, Berkeley, CA 94704

210–255. Managers of Nuclear Engineering of the following:

Alabama Power Company, 600 N. 18th Street, Birmingham, AL 35202
Arkansas Power and Light Company, 9th and Louisiana Street, Little Rock, AR 72203
Baltimore Gas and Electric Company, Gas and Electric Building, Charles Center, Baltimore, MD 21203
Bechtel Corporation, Gaithersburg, MD 20760
Boston Edison Company, 800 Boylston Street, Boston, MA 02199
Brown & Root, Inc., Houston, TX 77001
Carolina Power and Light Company, 336 Fayetteville Street, Raleigh, NC 27602
Cincinnati Gas and Electric, 139 E. Fourth Street, Cincinnati, OH 45201
Commonwealth Edison Company, P.O. Box 767, Chicago, IL 60690
Connecticut Yankee Atomic Power Company, P.O. Box 270, Hartford, CT 06101
Consolidated Edison Company, 4 Irving Place, New York, NY 10003
Consumers Power Company, 212 W. Michigan Avenue, Jackson, MI 49201
Detroit Edison Company, 2000 Second Avenue, Detroit, MI 48226
Duke Power Company, Charlotte, NC 28201
Duquesne Light Company, 435 Sixth Avenue, Pittsburgh, PA 15219
Florida Power Corporation, P.O. Box 14042, St. Petersburg, FL 33733
Florida Power and Light Company, 4200 Flagler Street, Miami, FL 33134
Georgia Power Company, 270 Peachtree Building, Atlanta, GA 30303
Gibbs & Hill, Inc., New York, NY 10001
Indiana and Michigan Electric Company, P.O. Box 18, Bowling Green Station, New York, NY 10004
Iowa Electric Light and Power Company, 823 Walnut Street, Des Moines, IA 50303
Jersey Central Power and Light Company, Madison Avenue at Punchbowl Road, Morristown, NJ 07960
Long Island Lighting Company, 250 Old County Road, Mineola, NY 11501
Maine Yankee Atomic Power Company, 9 Green Street, Augusta, ME 04330
Metropolitan Edison Company, P.O. Box 542, Reading, PA 19603
New York State Electric and Gas Corporation, Ithaca, NY 14850
Niagara Mohawk Power Company, 300 Erie Boulevard W., Syracuse, NY 13202
Northern Indiana Public Service Company, 5265 Hohman Avenue, Hammond, IN 46320
Northern States Power Company, 100 N. Barstow Street, Eau Claire, WI 54701
Nuclear Fuel Services, Inc., Rockville, MD 20852

Nuclear Fuels Services, West Valley, NY 14171
Pacific Gas and Electric Company, 77 Beale Street, San Francisco, CA 94106
Pennsylvania Power and Light, 901 Hamilton Street, Allentown, PA 18101
Philadelphia Electric Company, 1000 Chestnut Street, Philadelphia, PA 19105
Public Service Electric and Gas Company, 80 Park Place, Newark, NJ 07101
Rochester Gas and Electric Company, 89 East Avenue, Rochester, NY 14604
Sargent & Lundy Engineers, Chicago, IL 60603
Southern California Edison, P.O. Box 800, Rosemead, CA 91770
Stone & Webster Engineering Corporation, Boston, MA 02107
Toledo Edison Company, 420 Madison Avenue, Toledo, OH 43601
United Engineers and Constructors, Philadelphia, PA 19105
Vermont Yankee Nuclear Power Corporation, 77 Grove Street, Rutland, VT 05701
Virginia Electric and Power Company, 700 East Franklin Street, Richmond, VA 23261
Wisconsin Michigan Power Company, 231 W. Michigan Street, Milwaukee, WI 53201
Wisconsin Public Service, 700 N. Adams Street, Green Bay, WI 54305
Yankee Atomic Electric Company, 20 Turnpike Road, Westborough, MA 01581

256. H. G. Mangelsdorf, ACRS, Short Hills, NJ 07078
257. J. Marchaterre, Argonne National Laboratory, 9700 S. Cass Avenue, Argonne, IL 60439
258. C. L. Matthews, AEC, RDT, OSR, Oak Ridge National Laboratory
259. J. D. McAdoo, Westinghouse Electric Corporation, P.O. Box 355, Pittsburgh, PA 15230
260. J. E. McEwen, AEC, Division of Reactor Development and Technology, Washington, DC 20545
261. R. J. McWhorter, S. M. Stoller Corporation, New York, NY 10000
262. R. H. Meservey, Aerojet Nuclear Corporation, P.O. Box 1845, Idaho Falls, ID 83401
263. H. O. Monson, ACRS, Argonne National Laboratory, 9700 S. Cass Avenue, Argonne, IL 60439
264. J. B. Moore, Southern California Edison Company, P.O. Box 351, Los Angeles, CA 90053
265–266. H. Morewitz, Atomics International, P.O. Box 309, Canoga Park, CA 91304
267. R. L. Morgan, AEC-RDT Site Office, P.O. Box 1446, Canoga Park, CA 91304
268–270. P. A. Morris, Director, Division of Reactor Licensing, AEC, Washington, DC 20545
271. D. L. Morrison, Battelle Memorial Institute, 505 King Avenue, Columbus, OH 43201
272. C. Muehlhause, National Bureau of Standards, Washington, DC 20545

273. L. Murphy, U.S. Coast and Geodetic Survey, 4200 Connecticut Avenue, Washington, DC 20006
274. A. A. O'Kelley, ACRS, Littleton, CO 80120
275. D. Okrent, ACRS, Argonne National Laboratory, 9700 S. Cass Avenue, Argonne, IL 60439
276. Tetsuya Okuda, Kobe Steel, Ltd., Kobe, Japan
277. M. N. Ozisik, North Carolina State University, Department of Metallurgical Engineering, Raleigh, NC 27607
278–279. R. E. Pahler, AEC, Division of Reactor Development and Technology, Washington, DC 20545
280. N. J. Palladino, ACRS, Pennsylvania State University, University Park, PA 16802
281. J. F. Palmer, Chalk River Nuclear Laboratory, Atomic Energy of Canada, Ltd., Ontario, Canada
282. S. Paprocki, Battelle Memorial Institute, 505 King Avenue, Columbus, OH 43201
283. A. H. Peters, Savannah River Laboratory, E. I. du Pont de Nemours and Company, Aiken, SC 29802
284. R. Peterson, WADCO Corporation, P.O. Box 1970, Richland, WA 99352
285–286. N. Petrick, Westinghouse Electric Corporation, P.O. Box 158, Madison, PA 15663
287. G. B. Pleat, AEC, Division of Production, Washington, DC 20545
288. D. R. Poulter, UKAEA, Reactor Group Headquarters, Risley, Warrington, Lancaster, England
289–292. A. J. Pressesky, AEC, Division of Reactor Development and Technology, Washington, DC 20545
293. J. Proctor, Naval Ordnance Laboratory, White Oak, Silver Spring, MD 20900
294. J. W. Riches, Douglas United Nuclear, Richland, WA 99352
295. R. L. Ritzman, Battelle Memorial Institute, 505 King Avenue, Columbus, OH 43201
296. C. Robbins, Atomic Industrial Forum, Inc., New York, NY 10000
297. J.A.L. Robertson, Head, Reactor Materials Branch, Chalk River Nuclear Laboratory, Atomic Energy of Canada, Ltd., Ontario, Canada
298. T. Rockwell III, MPR Associates, Inc., 1140 Connecticut Avenue, Washington, DC 20006
299–300. J. B. Roll, Westinghouse NFD, Pittsburgh, PA 15230
301. D. Rose, Argonne National Laboratory, 9700 S. Cass Avenue, Argonne, IL 60439
302. M. Rosen, AEC, Division of Reactor Development and Technology, Washington, DC 20545
303. J. H. Russel, K Division, Los Alamos Scientific Laboratory, P.O. Box 1663, Los Alamos, NM 87544
304–305. M. F. Sankovich, Babcock & Wilcox Company, P.O. Box 1260, Lynchburg, VA 24505
306. W. Schikarski, Kernsforschungszentrum Karlsruhe, Institute fur Angewandte Reaktorphysik, Karlsruhe, Germany
307. V. E. Schrock, University of California, Institute of Engineering Research, Berkeley, CA 94704

308. R. Sevy, Argonne National Laboratory, 9700 S. Cass Avenue, Argonne, IL 60439
309. P. Shewmon, Argonne National Laboratory, 9700 S. Cass Avenue, Argonne, IL 60439
310. M. Siegel, General Electric Company, Pullman Way Facility, 80 Pullman Way, San Jose, CA 95111
311. C. P. Siess, ACRS, University of Illinois, Urbana, IL 61801
312. J. M. Simmons, AEC, Division of Reactor Development and Technology, Washington, DC 20545
313–316. W. Simmons, Argonne National Laboratory, 9700 S. Cass Avenue, Argonne, IL 60439
317. E. E. Sinclair, AEC, Division of Reactor Development and Technology, Washington, DC 20545
318. W. L. Smalley, AEC, Oak Ridge Operations Office, Oak Ridge, TN 37830
319–320. D. Spencer, Westinghouse Electric Corporation, P.O. Box 158, Madison, PA 15663
321. L. Squires, ACRS, 939 Nelson Walk, Naples, FL 33940
322. W. R. Stratton, ACRS, Los Alamos Scientific Laboratory, P.O. Box 1663, Los Alamos, NM 87544
323–324. R. Swanson, AEC, Idaho Operations Office, P.O. Box 2108, Idaho Falls, ID 83401
325. J. A. Swartout, Union Carbide Corporation, 270 Park Avenue, New York, NY 10000
326. W. A. Sutherland, General Electric Company, Pullman Way Facility, 80 Pullman Way, San Jose, CA 95111
327–330. S. A. Szawlewicz, AEC, Division of Reactor Development and Technology, Washington, DC 20545
331–332. J. Taylor, Westinghouse Electric Corporation, P.O. Box 158, Madison, PA 15663
333. M. F. Valerino, Combustion Engineering, Inc., Nuclear Division, P.O. Box 500, Windsor, CT 06095
334. S. Vandenberg, General Electric Company, Pullman Way Facility, 80 Pullman Way, San Jose, CA 95111
335–336. E. Veenard, Edison Electric Institute, New York, NY 10016
337. G. E. Wade, General Electric Company, Pullman Way Facility, 80 Pullman Way, San Jose, CA 95111
338. C. S. Walker, Tennessee Valley Authority, Knoxville, TN 37900
339. D. H. Walker, Aerojet Nuclear Corporation, P.O. Box 1845, Idaho Falls, ID 83401
340. R. Wascher, Babcock & Wilcox Company, P.O. Box 1260, Lynchburg, VA 24505
341. R. Waterfield, Division of Radiological and Environmental Protection, AEC, Washington, DC 20545
342. G. E. Watkins, Edison Electric Institute, New York, NY 10016
343. C. H. Waugman, Tennessee Valley Authority, Chattanooga, TN 37400
344. L. J. Weidner, Los Angeles Department of Water and Power, Los Angeles, CA 90000
345. J. F. White, General Electric Company, Nuclear Systems Programs, P.O. Box 15132, Cincinnati, OH 45215
346. M. J. Whitman, AEC, Division of Reactor Development and Technology, Washington, DC 20545

347. J. G. Wilhelm, Kernsforschungszentrum, Karlsruhe, Germany
348. B. Wolfe, WADCO Corporation, P.O. Box 1970, Richland, WA 99352
349. R. Wright, Argonne National Laboratory, 9700 S. Cass Avenue, Argonne, IL 60439
350. L. J. Ybarrondo, Aerojet Nuclear Corporation, P.O. Box 1845, Idaho Falls, ID 83401
351. J. O. Zane, Aerojet Nuclear Corporation, P.O. Box 1845, Idaho Falls, ID 83401
352. E. Zebroski, General Electric Company, 310 DeGuigne Drive, Sunnyvale, CA 94086
353. Laboratory and University Division, AEC, Oak Ridge Operations
354. Patent Office, AEC, Oak Ridge Operations
355–573. Given distribution as shown in TID-4500 under Reactor Technology category (25 copies – NTIS)